UNIVERSIDADE DE SÃO PAULO
ESCOLA POLITÉCNICA

DAVID ALEJANDRO LAZO VÁSQUEZ

Study on stability and flow-pattern transitions of stratified flows in pipes

São Paulo
2023

UNIVERSIDADE DE SÃO PAULO
ESCOLA POLITÉCNICA

DAVID ALEJANDRO LAZO VÁSQUEZ

Estudo de estabilidade e transição de padrão de escoamentos estratificados em tubulações

São Paulo
2023

DAVID ALEJANDRO LAZO VÁSQUEZ

Study on stability and flow-pattern transitions of stratified flows in pipes

Revised version

Doctoral thesis presented to the Graduate Program in Mechanical Engineering at Escola Politécnica, Universidade de São Paulo, to obtain the degree of Doctor of Science.

Concentration area:
Mechanical Engineering of Energy and Fluids

Supervisor:
Prof. Dr. Jorge Luis Baliño

São Paulo
2023

Este exemplar foi revisado e corrigido em relação à versão original, sob responsabilidade única do autor e com a anuência de seu orientador.

São Paulo, _____ de _____ de _____

Assinatura do autor: _____

Assinatura do orientador: _____

Catalogação-na-publicação

Lazo Vasquez, David Alejandro
Study on stability and flow-pattern transitions of stratified flows in pipes / D. A. Lazo Vasquez -- versão corr. -- São Paulo, 2023.
95 p.

Tese (Doutorado) - Escola Politécnica da Universidade de São Paulo. Departamento de Engenharia Mecânica.

1.Dinâmica dos Fluidos Computacional 2.Escoamento Bifásico 3.Estabilidade de Sistemas 4.Método dos Elementos Finitos I.Universidade de São Paulo. Escola Politécnica. Departamento de Engenharia Mecânica II.t.

This thesis is lovingly dedicated to my mother, Gloria.

ACKNOWLEDGEMENTS

I want to express my gratitude to my supervisor Jorge, without whose support I could not have undertaken this journey. This work was supported by *Coordenação de Aperfeiçoamento de Pessoal de Nível Superior* (CAPES), *Ministério das Relações Exteriores do Brasil* (MRE), *Programa de Estudantes-Convênio de Pós-Graduação* (PEC-PG), *Fundação de Desenvolvimento Tecnológico da Engenharia* (FDTE), and *Petróleo Brasileiro S.A.* (Petrobras).

ABSTRACT

LAZO VÁSQUEZ, D. A. **Study on stability and flow-pattern transitions of stratified flows in pipes**. 2023. Doctoral Thesis – Escola Politécnica, Universidade de São Paulo, São Paulo, 2023.

In the oil and gas industry, predicting multiphase flow pattern transitions plays an essential role. Two-phase flow pipeline systems are frequently simulated by solving the one-dimensional two-fluid model equations (i.e., cross-sectional average per phase of the three-dimensional Navier–Stokes equations) with first-order finite-volume methods. However, physical instabilities can be damped due to excessive numerical diffusion during wave growth. The Taylor-Hood finite elements have been employed for solving the Navier Stokes equations, mainly due to their numerical stability properties, circumventing the use of staggered grids, frequently used in the finite volume method. This thesis proposes a model to predict potential flow pattern transitions, considering gas-liquid stratified smooth flow as the initial condition, through the dynamic solution of the two-fluid model with Taylor-Hood elements for the spatial discretization combined with implicit time schemes. The differential equations are spatially discretized with a mixed formulation of higher-order continuous Galerkin elements for the average phase velocities and lower-order continuous Galerkin elements for the interfacial pressure and liquid holdup. By constructing fully discrete flow pattern maps, the model estimates neutral stability curves and well-posed limits through the simulation of liquid wave growth in time for a set of initial conditions and pipe inclinations. Overall, spatial discretization using Taylor-Hood mixed finite elements demonstrates a favorable ability to reproduce wave growth and predict flow pattern transitions. The model describes wave growth in different pipeline configurations for stratified smooth initial conditions within the Viscous Kelvin-Helmholtz region and under the well-posed limits. The effect of the initial conditions, mesh configuration, order of basis functions, and the influence of the local pipe inclination on stability has been investigated through a stiffness analysis of the semi-discretized equations and a Fourier analysis of the fully-discretized equations. The hybrid differential-discrete flow pattern maps based on Kelvin-Helmholtz instabilities and dynamic simulations depict the factual flow stability regions for a large set of initial conditions, enabling the prediction of potential ill-posedness and flow pattern transitions. The model is written in Python 3 and the Open Source FEniCS Project computing platform for the finite element method. The model enables the addition of regularization terms and other spatial and time discretization schemes for further studies.

Computational Fluid Dynamics, Finite-element Method, Gas-liquid flow, Linear stability, Taylor-Hood elements.

RESUMO

LAZO VÁSQUEZ, D. A. **Estudo de estabilidade e transição de padrão de escoamentos estratificados em tubulações**. Tese – Escola Politécnica, Universidade de São Paulo, São Paulo, 2023.

A previsão de transição de padrão de escoamentos multifásicos é essencial na indústria de óleo e gás. Sistemas multifásicos em linhas longas são frequentemente simulados com o modelo unidimensional de dois fluidos, que consiste em uma média da seção transversal por fase das equações de *Navier-Stokes*. É comum usar métodos de volumes finitos de primeira ordem para resolver as equações; no entanto, com métodos de discretização de baixa ordem, instabilidades físicas podem ser atenuadas devido à difusão numérica excessiva durante o crescimento de ondas. Esta tese propõe um modelo capaz de prever potenciais transições de padrão de escoamento através da solução dinâmica do modelo de dois fluidos com elementos finitos do tipo *Taylor-Hood* para a discretização espacial, combinado com esquemas temporais implícitos. Ultimamente, os elementos finitos do tipo *Taylor-Hood* têm sido utilizados para resolver as equações de *Navier-Stokes* devido às suas propriedades de estabilidade numérica, evitando o uso de malhas deslocadas, prática comum no método dos volumes finitos. Neste estudo, as equações diferenciais são discretizadas espacialmente com uma formulação mista de: elementos do tipo Continuo *Galerkin* de alta ordem para as velocidades das fases e Continuo *Galerkin* de baixa ordem para a pressão interfacial e a altura de líquido. Através de mapas de padrão de escoamento baseados nas equações totalmente discretizadas, o modelo estima as curvas de estabilidade neutra e limites de um problema bem posto mediante a simulação do crescimento de ondas de líquido para escoamentos estratificados lisos dentro da região *Kelvin-Helmholtz* Viscosa e do limite de um problema bem posto. O efeito das condições iniciais, configuração de malha e a influência da inclinação da tubulação são investigadas mediante a análise de estabilidade das equações semi-discretizadas e a análise de *Fourier* das equações totalmente discretizadas. Os mapas de padrão de escoamento híbridos (equações diferenciais, equações discretizadas e de dados da literatura), baseados em instabilidades *Kelvin-Helmholtz* e simulações dinâmicas, mostram as regiões de estabilidade para o conjunto de condições analisado. O modelo está escrito em *Python* 3 e a plataforma de código aberto para métodos de elementos finitos *FEniCS Project*. O modelo permite a adição de termos de regularização ou outros métodos de discretização espacial e temporal para futuros estudos.

Palavras-chave: Elementos finitos tipo *Taylor-Hood*, Escoamento Gás-líquido, Estabilidade Linear, Método dos Elementos Finitos, Mecânica dos Fluidos Computacional.

LIST OF FIGURES

LIST OF TABLES

LIST OF ABBREVIATIONS AND ACRONYMS

Acronym	Description
A	Annular flow
ARPACK	Arnoldi package
BDF1	First order backward differentiation formula (implicit Euler scheme)
BDF2	Second order backward differentiation formula (implicit Euler scheme)
CD	Central differences scheme
CFD	Computational fluid dynamics
CFL	Courant–Friedrichs–Lewy
CG_q	Continuous Galerkin elements of degree q
CN	Crank-Nicolson scheme
D	Dispersed flow
DFPM	Discrete flow pattern map
IKH	Inviscid Kelvin-Helmholtz
LBB	Ladyzhenskaya–Babuška–Brezzi (inf-sup condition)
I	Intermittent flow
PETSc	Portable, Extensible Toolkit for Scientific Computation
SS	Stratified smooth flow
SW	Stratified wavy flow
TFM	Two-fluid model
TH	Taylor-Hood
UMFPACK	Unsymmetric MultiFrontal method
VKH	Viscous Kelvin-Helmholtz

LIST OF SYMBOLS

Roman Symbols

Symbol	Description	Dimension	SI unit
A	pipe cross-sectional area	L^2	m^2
$\mathbf{A}$	Matrix of coefficients of the local term	-	-
A_g	gas phase area	L^2	m^2
A_l	liquid phase area	L^2	m^2
a	bilinear form of the variational equation	-	-
a_0	parameter for time integration (2.29)	-	-
a_1	parameter for time integration (2.29)	-	-
a_2	parameter for time integration (2.29)	-	-
$\mathbf{B}$	Matrix of coefficients of the convective term	-	-
B	Bubble element	-	-
$\mathbf{C}$	Matrix of coefficients of the source term	-	-
C_{CFL}	Courant–Friedrichs–Lewy (CFL) convergence condition	-	-
c_g	speed of sound in air	LT^{-1}	$m\ s^{-1}$
$\bar{d}$	corrected diameter	L	m
d	pipe diameter	L	m
f_{gl}	gas-liquid interfacial empirical friction factor correlation	-	-
f_g	gas phase empirical friction factor correlation	-	-
f_l	liquid phase empirical friction factor correlation	-	-
g	gravitational acceleration	LT^{-2}	$m\ s^{-2}$
H	height of the duct	L	m
h_l	height of the liquid phase	L	m
I	imaginary unit	$I = \sqrt{-1}$	
Im	imaginary component	-	-
J_ϕ	generic diffusion flux	$\mathsf{ML}^{-2}\mathsf{T}$	$kg\ m^{-2}\ s$
k	generic phase	-	-
k	wavenumber	L^{-1}	m^{-1}
L	length of the pipe	L	m
L	linear form of the variational equation	-	-
N	number of elements	-	-
$P_{k\phi}$	generic wetted perimeter	L	m
P_{gw}	gas phase wetted perimeter	L	m
P_{lw}	liquid phase wetted perimeter	L	m

P_{gl}	gas-liquid interface perimeter	L	*m*
p	order of the basis functions	-	-
p_i	interfacial pressure	$ML^{-1}T^{-2}$	*Pa*
Re	real component	-	-
r	eigenvector	-	-
s	an arbitrary (x, y) location	-	-
q	dimension of the vector of the primitive variables	-	-
t	time	T	*s*
U	vector of conserved variables $\mathbf{U} \in \mathbb{R}^{qN}$	-	-
$\widetilde{\mathbf{U}}$	vector of the perturbed primitive variables	-	-
u	velocity	LT^{-1}	$m\ s^{-1}$
u_g	gas velocity	LT^{-1}	$m\ s^{-1}$
u_l	liquid velocity	LT^{-1}	$m\ s^{-1}$
u_{sg}	superficial gas velocity	LT^{-1}	$m\ s^{-1}$
u_{sl}	superficial liquid velocity	LT^{-1}	$m\ s^{-1}$
V	finite element space	-	-
v	test function	-	-
W	vector of the primitive variables $\mathbf{W} \in \mathbb{R}^q$ (q = 4)	-	
$\widehat{\mathbf{W}}$	amplitude of wave-like solutions	-	-
$\widetilde{\mathbf{W}}$	vector of the perturbed primitive variables	-	-
w	trial function	-	-
x	The Easting geographic coordinate	-	-
y	The Northing geographic coordinate	-	-

Greek Symbols

Symbol	Description	Dimension	SI unit
α	volume fraction	-	-
β	pipe inclination	-	*rad*
γ	stratification angle	-	*rad*
δ	infinitesimal	-	-
ϵ	pipe roughness	L	*m*
ε	amplitude of the traveling wave	L	*m*
λ	wavelength	L	*m*
μ	dynamic viscosity	$M\ L^{-1}\ T^{-1}$	$kg\ m^{-1}\ s^{-1}$
Ω	element space	-	-
ω	angular frequency	T^{-1}	s^{-1}
$\partial\Omega$	surface of the finite element space	-	-

ρ	density	ML^{-3}	$kg\ m^{-3}$
σ	surface tension	$\mathrm{M\ L}^{-1}\ \mathrm{T}^{-2}$	$N\ m^{-2}$
τ	shear stress	$\mathrm{M\ L}^{-1}\ \mathrm{T}^{-2}$	$N\ m^{-2}$
$\bar{\tau}$	local truncation of temporal schemes		
θ	parameter for time integration in (2.29)	-	-

Subscripts

Subscript	Description
0	initial
g	gas
h	hydraulic
i	interfacial
l	liquid
q	order of the basis functions
ϕ	generic phase or wall
s	an arbitrary (x, y) location
q	order of the basis functions
w	wall
x	easting geographic coordinate
y	northing geographic coordinate

Superscripts

Superscript	Description
in	inlet of the spatial domain
n	n^{th} time step
n − 1	previous time step
n + 1	future time step
out	outlet of the spatial domain

Dimensionless Numbers

Number	Description
Re	Reynolds number

CONTENTS

1 INTRODUCTION AND BACKGROUND

1.1 Stratified and intermittent flow in pipelines

In the petroleum industry (see Figure 1), oil and gas are transported through long multiphase pipeline systems (Zwieten et al., 2017) presenting different phase distributions depending on several parameters (i.e., phase velocities, densities, viscosities, and pipe configurations) (Smith, 2017). Under operation conditions, stratified and intermittent flow patterns are the most frequent. Figures 2 to 4 illustrate the flow patterns found in the oil and

Figure 1 – Christmas tree, manifold, and risers in the Petrobras (Brazil) offshore oil production systems.

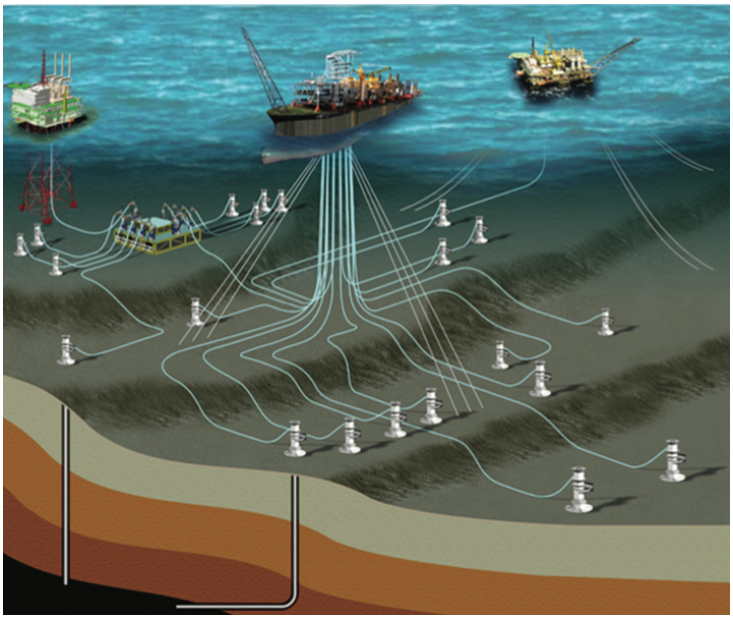

Note: adapted from Morais (2013).

gas industry. At low flow rates and mainly at horizontal and downhill sections, in stratified flow, the gas and the liquid are separated into different layers, with the gas flowing above the liquid phase (Schlumberger, 2020). The liquid level rises as the liquid flow rate increases and a wave is formed. Perturbations of short waves may grow into larger and longer ones as a result of pipe undulations (Issa; Kempf, 2003) and Kelvin–Helmholtz (KH) instabilities (Lin; Hanratty, 1986; Z.Fan; Ruder; Hanratty, 1993; Ansari, 1998).

Slug flow consists of aerated liquid plugs followed by gas bubbles (i.e., Taylor Bubbles). Slugs may grow if their fronts travel faster than their tails, and, alternatively, they would collapse (Taitel; Barnea, 1990; Zheng; Brill; Taitel, 1994; Issa; Kempf, 2003). The emergence of slugs can yield fluctuations of pressure and severe production decrements. Consequently, the prediction of slug flow considerably influences the sizing of receiving facilities, e.g., slug catchers or separators (Taitel; Barnea, 1998; Zwieten et al., 2017).

Figure 2 – Stratified flow patterns in horizontal and slightly inclined pipes.

(a) Smooth flow (SS). (b) Wavy flow (SW). (c) SW (higher u_g).

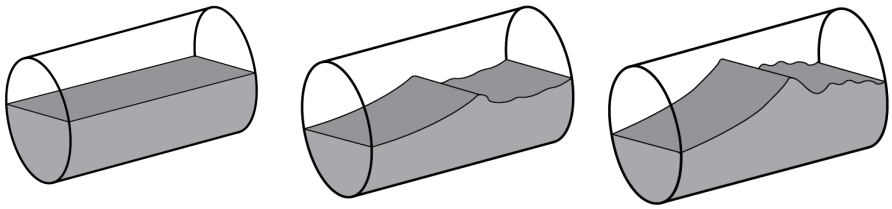

Note: the gas velocity is denoted by u_g. Adapted from Montini (2010).

Figure 3 – Intermittent (I) flow patterns in horizontal and inclined pipes.

(a) Elongated bubble flow. (b) Slug flow.

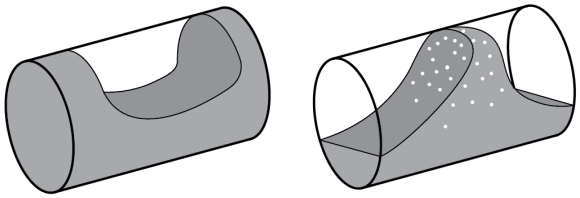

Note: adapted from Montini (2010).

Figure 4 – Annular and Dispersed (AD) flow patterns in horizontal and inclined pipes.

(a) Annular flow. (b) Dispersed flow.

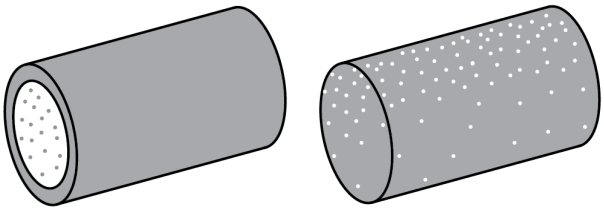

Note: adapted from Montini (2010).

Taitel and Dukler (1976) constructed phenomenological flow pattern maps for steady two-phase flows in horizontal and nearly horizontal pipes to study the influence of the pipe diameter, viscosity, and local inclination on flow pattern transitions. Some authors have built flow pattern maps for different pipe configurations, which include horizontal and slightly inclined pipes (Taitel; Dukler, 1976; Husain; WG, 1978; Lin; Hanratty, 1986), vertical upward flow (Taitel et al., 1980; Ishii, 1975; McQuillan; Whalley, 1985), inclined upward flow (Barnea et al., 1985), downward inclined low (Barnea; Shoham; Taitel, 1982), amongst others. Figure 5 depicts flow pattern maps for steady-state water-air flow in horizontal and inclined straight pipes.

Figure 5 – Flow patterns in horizontal and nearly inclined straight pipes

(a) Horizontal.

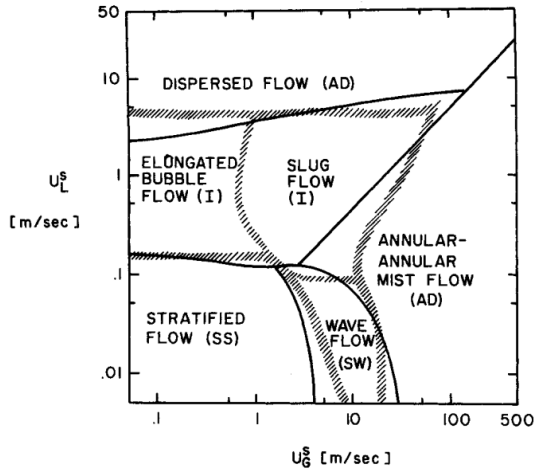

(b) Upward flow.

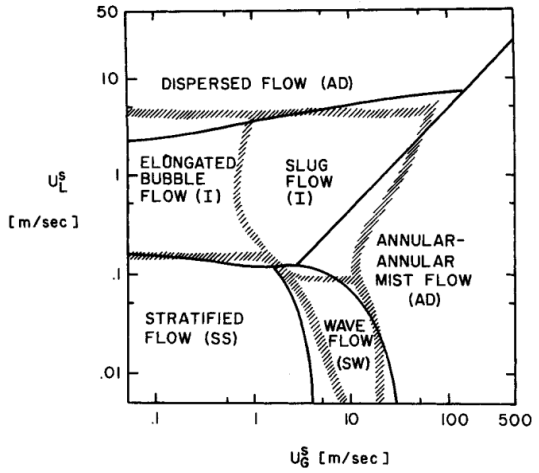

(c) Downward flow.

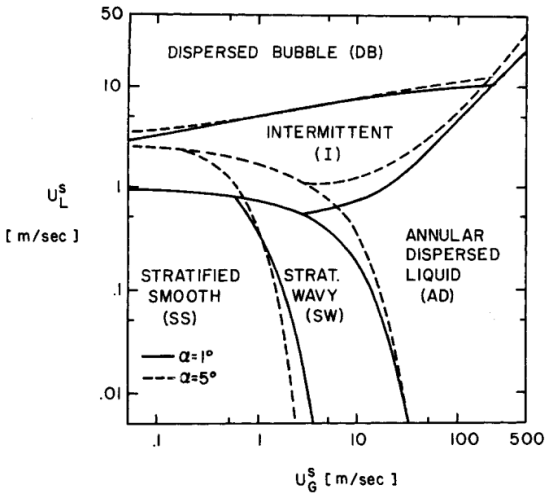

Note: The liquid and gas superficial velocities are represented by $u_L^s = u_l \alpha_l$ and $u_G^s = u_g \alpha_g$, respectively. From Taitel and Dukler (1976).

Theoretical flow patterns map may not be accurate enough to describe transient flow transitions. Experimentally, the initiation of slugging can occur above or below these boundaries (Shoham, 1982); consequently, slug initiation is one of the challenges in the multiphase flow simulation. One of the numerical techniques for predicting stratified to intermittent flow transitions is the Slug Capturing approach of Issa and Kempf (2003), which consists of the numerical simulation of the natural growth of instabilities, the formation of slugs, and the procession of slug trains. Slugging initiates automatically from numerical truncation, machine round-off in the computations, or starting from a non-equilibrium flow. When the liquid phase blocks the pipe, the gas equations vanish and transition criteria should be imposed (Bonzanini; Picchi; Poesio, 2017; Ferrari; Bonzanini; Poesio, 2017). According to Smith (2017), the Slug Capturing approach can be significantly slower due to the fine grid and reduced time step, so evaluating the feasibility of numerical methods for improving the prediction of the onset of slugging is decisive.

1.2 One-dimensional two-fluid model

The one-dimensional Two-fluid Model (Ishii, 1975) (hereafter Two-fluid Model) results from applying cross-sectional averaging per phase of the three-dimensional Navier–Stokes equations. For oil and gas systems, the numerical solution of the three-dimensional equations would be costly, considering the multi-scale nature of the problem (i.e., pipelines of the order of kilometers and gas bubbles of millimeters) (Zwieten et al., 2017). Therefore, despite its limitations (e.g. the absence of radial curvature for liquid liquid flows), the one-dimensional Two-fluid Model is frequently employed for simulating two-phase flows in pipelines.

The well-posedness of the Two-fluid Model equations has been studied by several authors (Pokharna; Mori; Ransom, 1997; Ansari, 1998; Issa; Kempf, 2003; Montini, 2010; Sanderse; Smith; Hendrix, 2017). The Two-fluid Model can become ill-posed and yield grid-dependent solutions for large relative superficial velocities (i.e., $u_r = |u_{sl} - u_{sg}|$). Above the limit of well-posedness, the Two-fluid Model has complex characteristics (Dinh; Nourgaliev; Theofanous, 2003) (i.e., the wave growth rates increase unboundedly as the wavelength shrinks to zero). The ill-posedness of the Two-fluid Model is still an open question (Holmås et al., 2008; Liao; Mei; Klausner, 2008; Fullmer et al., 2010; Bertodano et al., 2017; Sanderse; Smith; Hendrix, 2017). Several authors proposed different approaches to deal with the ill-posedness of the Two-fluid Model, which may be rendered well-posed, including appropriate short-wavelength physics. Pokharna, Mori and Ransom (1997), Montini (2010), Bertodano, Fullmer and Vaidheeswaran (2013) studied lower-order regularization of the Two-fluid Model (i.e., interfacial drag and hydrostatic pressure).

Ramshaw and Trapp (1978), Holmås et al. (2008), Montini (2010), Bonzanini, Picchi and Poesio (2017) studied higher-order regularization mechanisms (i.e., surface tension term (Ramshaw; Trapp, 1978; Pokharna; Mori; Ransom, 1997), artificial interfacial pressure terms (Evje; Flåtten, 2003; Fullmer et al., 2014; Liao; Mei; Klausner, 2008), and numerical diffusion terms (Holmås et al., 2008; Fullmer et al., 2014)). Including higher-order regularization terms leads to dispersive equation systems (i.e., waves of different wavelengths propagate at different phase velocities) (Montini, 2010). Surface tension can also make the equation system well-posed and introduce a cut-off wavelength (Ramshaw; Trapp, 1978). However, the maximum wave growth rates are still high.

Industrial codes render well-posedness by introducing diffusive terms to dampen the short-wavelength components of the numerical solution (i.e., numerical diffusion correlations serve as filters, rendering dissipation and stability). This strategy succeeds because of the "turbulent energy cascade," where the long-wavelength motion governs the energy dissipation rate. Using diffusion terms as regularization parallels the methods for modeling turbulent flow, where the small-scale eddies are not directly resolved (Bertodano et al., 2017). Montini (2010) investigated values to obtain representative pipe diameter cut-off wavelengths for different initial conditions.

1.3 Numerical modeling of stratified flow, wave growth, and slugging

The industry has proposed commercial codes (e.g., OLGA (Bendiksen et al., 1987; Bendlksen et al., 1991) and PLAC (Black et al., 1990)) to come up with solutions to the Two-fluid Model. In OLGA and PLAC, initially developed by the nuclear industry, fast transients correlated with Loss Of Coolant Accidents (LOCA) are of particular interest. In contrast, the petroleum industry is interested in slow transients associated with transporting and releasing slugs at receiving facilities (Masella et al., 1998).

Regarding academic formulations, the Two-fluid Model is frequently spatially discretized with first-order Finite Differences or Finite Volume schemes (Ansari; Shokri, 2011; Kim; Kang; Lowengrub, 2004; Kjeldby; Nydal, 2013; Liao; Mei; Klausner, 2008; Holmås et al., 2008; Fullmer, 2014; Ortega; Nieckele, 2005) and implicit time integration schemes. Some Slug Capturing codes (e.g., TRIOMPH (Issa; Kempf, 2003)) use first-order central difference schemes for the convective quantities to avoid the attenuation of physical instabilities due to excessive numerical diffusion (Liao; Mei; Klausner, 2008). Additionally, upwind schemes may present unfavorable stability properties (Fullmer, 2014) and high numerical diffusion. Moreover, Holmås et al. (2008) used a pseudo-spectral Fourier method to solve the Two-fluid Model. They indicated that the computational time is several orders of magnitude larger than that of classical finite difference schemes. Fullmer (2014) show improved accuracy of a second-order method over a first-order method. However, their approach leads to non-monotone results.

Sanderse, Smith and Hendrix (2017) studied the effect of the discretization schemes on the factual stability of the flow in horizontal pipes. They presented stability and ill-posedness regions through discrete flow pattern maps (DFPM) based on Kelvin-Helmholtz instabilities. Lately, Ferrari, Bonzanini and Poesio (2017) proposed a five-equation Two-fluid Model. They added a transport equation for the gas volumetric fraction to deal with ill-posedness. This equation indicates that the gas volumetric fraction is transported with the mean interfacial velocity (Drew, 1983; Munkejord; Gran, 2009; Ansari; Daramizadeh, 2012).

Zwieten et al. (2017) proposed an h-adaptive space-time Discontinuous-Galerkin Finite Element Method (DGFEM) scheme for simulating stratified flow within the well-posed region in horizontal pipes. For smooth initial problems, the DG method converges with the theoretical rate. Recently, Bezchlebová et al. (2019) used level set methods for modeling the interface of two-phase flows of immiscible fluids. They adopted Taylor-Hood (TH) elements for the transport equations and DG elements for the level-set equation.

1.4 Objective and contribution

This thesis aims to develop a hybrid stability and numerical model for predicting wave growth and the consequent potential flow pattern transitions in horizontal and slightly inclined pipes. The Two-fluid Model is numerically solved with finite elements. The contribution of

this work lies in a code that can be suited for two-phase flow simulations under different initial conditions and pipe configurations, enabling the investigation of numerical methods and regularization techniques. The numerical formulation is based on an adaptation of the techniques frequently used for solving convection-dominated problems with Taylor-Hood elements.

1.5 Outline of the thesis

This thesis is organized as follows. Chapter 1 describes the physical mechanisms that lead to slugging. Additionally, the background is shaped based on the state-of-the-art numerical modeling of two-phase flow. Chapter 2 presents the governing equations and the closure models. This chapter also details the numerical methods, the well-posedness analysis, the linear stability analysis, and the methods to construct differential and discrete flow pattern maps. Also, this chapter describes the numerical methods and their verification procedure. Chapter 3 discusses the most relevant results through eigenspectrum and flow pattern maps. The results of the validation and verification processes are also presented in this chapter. Chapter 4 details this work's conclusions and future perspectives.

2 METHODS

This chapter describes the governing equations, stability analysis, and the numerical formulation for predicting flow pattern transitions. The Two-fluid Model is solved through the finite element method, starting from stratified smooth flows as initial conditions.

2.1 Governing equations

2.1.1 Two-fluid Model

The one-dimensional Two-fluid Model (Ishii, 1975) consists of three conservation equations for each phase (i.e., mass, momentum, and energy). For isothermal flow, the energy equations can be dismissed. The mass and momentum conservation equations are given by:

$$\partial_t \left(\alpha_l \rho_l\right) + \partial_{\mathbf{s}} \left(\alpha_l \rho_l u_l\right) = 0 \tag{2.1}$$

$$\partial_t \left(\alpha_g \rho_g\right) + \partial_{\mathbf{s}} \left(\alpha_g \rho_g u_g\right) = 0 \tag{2.2}$$

$$\begin{aligned} \partial_t \left(\alpha_l \rho_l u_l\right) + \partial_{\mathbf{s}} \left(\alpha_l \rho_l u_l^2\right) + \alpha_l \partial_{\mathbf{s}} p_{il} + \alpha_l \rho_l g \partial_{\mathbf{s}} h_l \cos\beta \\ = -\alpha_l \rho_l g \sin\beta - F_{lw} + F_{gl} \end{aligned} \tag{2.3}$$

$$\begin{aligned} \partial_t \left(\alpha_g \rho_g u_g\right) + \partial_{\mathbf{s}} \left(\alpha_g \rho_g u_g^2\right) + \alpha_g \partial_{\mathbf{s}} p_{ig} + \alpha_g \rho_g g \partial_{\mathbf{s}} h_l \cos\beta \\ = -\alpha_g \rho_g g \sin\beta - F_{gw} + F_{lg} \end{aligned} \tag{2.4}$$

The independent variables α, u, and p_i represent the volumetric fraction, phase velocity, and interfacial pressure. The subscripts l and g indicate the liquid and gas phases. The remaining variables β and F represent the local inclination of the pipeline with respect to the horizontal and the shear force, respectively. Time is represented by t, and s is the spatial coordinate. Figure 6 illustrates the parameters of stratified flows in horizontal and inclined straight pipes.

Figure 6 – Stratified flow layout

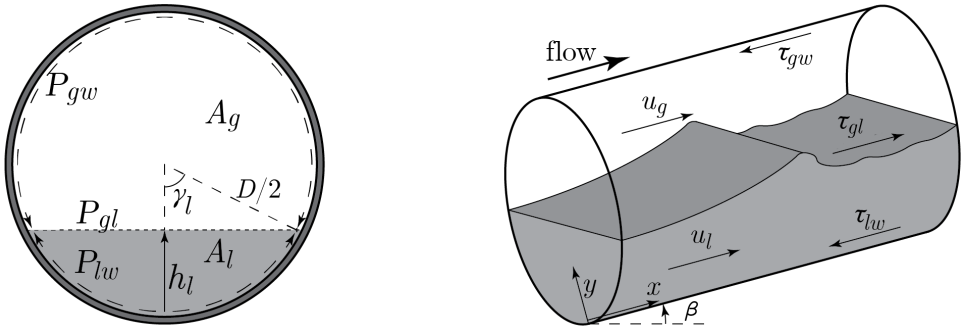

Note: adapted from Montini (2010).

The interfacial pressure is defined by p_i, the liquid and gas volumetric fractions sum to one $\alpha_l + \alpha_g = 1$, and the average phase velocities u_{sl} and u_{sg}can be expressed as functions of the volumetric fractions:

$$u_l = \frac{u_{sl}}{\alpha_l}, \quad u_g = \frac{u_{sg}}{\alpha_g} \tag{2.5}$$

The liquid density is constant, and the gas density ρ_g is related to the interfacial pressure p_i by the correlation of Montini (2010):

$$\rho_g = \frac{p_i - p_{i,0}}{c_{g,0}^2} + \rho_{g,0} \tag{2.6}$$

where $c_{g,0}$, $p_{i,0}$, and $\rho_{g,0}$ represent the propagation velocity of an infinitesimal pressure wave compatible with an isothermal evolution, the atmospheric pressure, and the air density at atmospheric pressure, respectively.

Equations (2.1) - (2.4) can be written in a matrix (quasi-linear) form:

$$\mathbf{A}(\mathbf{W})\partial_t \mathbf{W} + \mathbf{B}(\mathbf{W})\partial_{\mathbf{s}} \mathbf{W} + \mathbf{C}(\mathbf{W}) = 0 \tag{2.7}$$

where $\mathbf{W} = [\alpha_l, u_l, u_g, p]^{\mathsf{T}} \in \mathbb{R}^q$ is a column vector of the primitive variables. The matrices **A** and **B** are the Jacobian matrices of dimension n x n. The column vector that contains the source terms is denoted by **C**, and n is the number of independent variables. The matrices $\mathbf{A}$ and $\mathbf{B}$, and the vector $\mathbf{C}$ are detailed in Appendix 4.2.

Equations (2.1)-(2.4) are discretized with Taylor-Hood finite element methods and implicit time schemes. The transient equations are resolved for a set of initial conditions in distinct pipe configurations as follows.

2.1.2 Closure relations

2.1.2.1 Geometry

The direction of τ_{gl} shown in Fig. 6 is given by:

$$sgn\ (\tau_{k\theta}) = \begin{cases} 1 & \text{if} \quad u_g > u_l, \\ 0 & \text{if} \quad u_g = u_l, \\ -1 & \text{if} \quad u_g < u_l \end{cases} \tag{2.8}$$

where $k \in \{l, g\}$ denotes a phase, $\theta \in \{l, g, w\}$ and $k \neq \theta$.

According to Biberg (1999), the geometric relation between the stratification angle γ_l and the liquid volumetric fraction α_l reads:

$$\gamma_l = \pi\left(\alpha_l\right) + \left(\frac{3\pi}{2}\right)^{1/3}\left(1 - 2\alpha_l + \alpha_l^{1/3} - (1-\alpha_l)^{1/3}\right) \tag{2.9}$$

The cross-sectional areas of the phases are defined by $A_k = \alpha_k A$. The following geometric identities are used to express the wall and interfacial perimeters in terms of the stratification angle:

$$P_{lw} = D\gamma_l \tag{2.10}$$

$$P_{gw} = D(\pi - \gamma_l) \tag{2.11}$$

$$P_{gl} = D \sin \gamma_l \tag{2.12}$$

Finally, the liquid height h_l and the liquid holdup α_l in the hydrostatic pressure term are related by the expression of Bonizzi (2003):

$$\partial_{\mathbf{s}} h_l \cos \beta = d_c \partial_{\mathbf{s}} (1 - \alpha_l) \tag{2.13}$$

The corrected diameter reads:

$$d_c = -\frac{\pi d \cos \beta}{4 \sin (\gamma_l / 2)} \tag{2.14}$$

and γ_l is the stratification angle.

2.1.2.2 Friction models

The shear stress terms are physically modeled by:

$$\tau_{k\phi} = \begin{cases} \frac{1}{2} f_{k\phi} \rho_k u_k |u_k| & \text{if} \quad \phi = w, \\ \frac{1}{2} f_{k\phi} \rho_g (u_k - u_\phi) |u_k - u_\phi| & \text{if} \quad \phi \in \{g, l\} \end{cases} \tag{2.15}$$

where the subscript $k \in \{l, g\}$. The Fanning friction factors are denoted by f_l, f_g, and f_{gl} (see Table 1) based on the combination proposed in Issa and Kempf (2003), Montini (2010).

Table 1 – Correlations for the friction factors

	Laminar flow $(Re_k < 1180)$	Turbulent flow $(Re_k \geq 1180)$	Source
f_{lw}	$24\, Re_l^{-1}$	$0.0262\ (\alpha_1 Re_l)^{-0.139}$	Hand (1991), Balay et al. (1997)
f_{gw}	$16\, Re_g^{-1}$	$0.046\, Re_g^{-0.2}$	Taitel and Dukler (1976)
$f_{gl} = f_{lg}$	$16\, Re_g^{-1}$	$\max\{f_{gw}, 0.014\}$	Liao, Mei and Klausner (2008)

The subscripts $k \in \{l, g\}$ and w represents the pipe wall.

The Reynolds numbers are evaluated as in Issa and Kempf (2003):

$$Re_g = \frac{D_{hg} u_g \rho_g}{\mu_g} \tag{2.16}$$

$$Re_l = \frac{D u_{sl} \rho_1}{\mu_1} \tag{2.17}$$

where the hydraulic diameter for the gas phase is evaluated as in Agrawal, Gregory and Govier (1973):

$$D_{hg} = \frac{4 A_g}{P_{gw} + P_{gl}} \tag{2.18}$$

2.2 Numerical method

2.2.1 Spatial discretization

2.2.1.1 Variational form

For a domain $\Omega \subset \mathbb{R}^n$ with boundaries $\partial\Omega = \Gamma_D^{in} \cup \Gamma_D^{out}$, the quasi-linear form of the governing equations reads:

$$\partial_t \mathbf{W} + \mathbf{B}(\mathbf{W})\partial_{\mathbf{s}}\mathbf{W} + \mathbf{C}(\mathbf{W}) = 0 \quad \text{in} \quad \Omega \tag{2.19}$$

with the Dirichlet boundary conditions

$$\mathbf{W} = \mathbf{W}\,(0,t) \quad \text{on} \quad \Gamma_D^{in} \tag{2.20}$$

$$\mathbf{W} = \mathbf{W}\,(L,t) \quad \text{on} \quad \Gamma_D^{out} \tag{2.21}$$

where Γ_D^{in} is defined by the liquid volumetric fraction and the velocities, and Γ_D^{out} by the interfacial pressure. The Two-fluid Model (i.e., 2.1 to 2.4) can be formulated in a mixed variational form, where the four variables α_l, u_l, u_g, p_i are approximated simultaneously by the following problem:

Find $\mathbf{W_h} = [\alpha_l, u_l, u_g, p_i]^T$ in V_h such that:

$$a\,(\mathbf{W}_h, \mathbf{V}_h) = L\,(\mathbf{V}_h) \tag{2.22}$$

$$R\,(\mathbf{W}_h, \mathbf{V}_h) = a_A\,(\mathbf{W}_h, \mathbf{V}_h) - L\,(\mathbf{V}_h) = 0 \tag{2.23}$$

where $L\,(\mathbf{V}_h)$ is the linear form, $a\,(\mathbf{W}_h, \mathbf{V}_h)$ is the bilinear form, and $R\,(\mathbf{W}_h, \mathbf{V}_h)$ is the residual. The mixed function space $V_h = V_{h,1} \times V_{h,2} \times V_{h,3} \times V_{h,4}$ is composed of scalar-valued continuous piecewise polynomials.

For the test functions $[v_1, v_2, v_3, v_4]^{\mathsf{T}} \in V_h$ and trial functions $w_1, w_2, w_3, w_4 \in V_h$ the variational form reads:

$$\sum_{\Omega \in \Omega_h} \int_\Omega \partial_t \mathbf{W}_h \mathbf{V}_h \mathrm{d}x + \sum_{\Omega \in \Omega_h} \int_\Omega \mathit{a}_A\left(\mathbf{B}_{\mathbf{0},h}; \mathbf{W}_h, \mathbf{V}_h\right) \mathrm{d}x := \sum_{\Omega \in \Omega_h} \int_\Omega \mathbf{C}_{\mathbf{0},h} \mathrm{d}x \tag{2.24}$$

where the discretized vector of variables is:

$$\mathbf{W_h} = \left[(\mathbf{W_{h1}})_{1,\ldots,N}, (\mathbf{W_{h2}})_{1,\ldots,N}, (\mathbf{W_{h3}})_{1,\ldots,N}, (\mathbf{W_{h4}})_{1,\ldots,N}\right]^T \tag{2.25}$$

A weighted residual method resolves equation (2.24). The approximate solution is a linear combination of basis functions in a finite subspace $V_h \subset V$. The approximate solution is a sum of coefficients times basis functions:

$$\mathbf{W_h}(s,t) \approx W_h(s,t) = \sum_N^{j=1} \xi_j \phi_j(x,t)), V_h = \{\phi_1, ..., \phi_N\}\,\{\phi_j\}_{j=1}^N \tag{2.26}$$

The coefficients $\{\xi_j\}_{j=1}^{N}$ is determined by an orthogonal projection of the residual of the equation system onto the finite subspace V_h, that is:

$$R\left(W_h, V_h\right) = 0 \tag{2.27}$$

for all $v \in V_h$, which corresponds to a matrix equation $Ax = b$, that is solved by numerical methods.

The advection term a_A is:

$$\sum_{\Omega \in \Omega_h} \int_{\Omega} a_A\left(\mathbf{B}_{\mathbf{0},h}; \mathbf{W}_h, \mathbf{V}_h\right) = \sum_{\Omega \in \Omega_h} \int_{\Omega} \mathbf{V}_h . \nabla \mathbf{B}_{\mathbf{0},h} \mathbf{W}_h \mathrm{d}x, \tag{2.28}$$

2.2.1.2 Taylor-Hood mixed finite elements

The Two-fluid Model (i.e., Eqs. (2.1) to (2.4)) represents a convection-dominated problem, and the diffusive forces are introduced as sources. Taylor and Zienkiewicz (2013) pointed out that the numerical treatment of convection-dominated equations is non-trivial. The Two-fluid Model equations are frequently resolved with first-order Finite-Diferences or the Finite Volume method, using staggered grids (Ansari; Shokri, 2011; Kim; Kang; Lowengrub, 2004; Kjeldby; Nydal, 2013; Liao; Mei; Klausner, 2008; Holmås et al., 2008; Fullmer, 2014; Ortega; Nieckele, 2005), usually presenting excessive numerical diffusion for higher-order schemes. Finite Difference and Finite Volume methods need staggered grids for the variables (Versteeg; Malalasekera, 2007). Volume quantities (i.e., volumetric fraction, interfacial pressure) are stored at cell centroids (ordinary nodes), and velocities are stored at cell faces (staggered grid) (Anderson; Tannehill; Pletcher, 1997; Versteeg; Malalasekera, 2007; Montini, 2010).

The Model resolves Eqs. (2.1) to (2.4) with continuous finite elements for the spatial discretization due to their accuracy and stability since the initial conditions are smooth (Alnæs et al., 2014). Logg, Mardal and Wells (2012) presented element spaces frequently used for resolving the Navier-Stokes equations (e.g., Taylor–Hood (Taylor; Hood, 1973; Boffi, 1997) and MINI elements, a cheaper alternative to Taylor-Hood (Arnold; Franco; Fortin, 1984)).

The Taylor-Hood elements (Taylor; Hood, 1973; Boffi, 1997) used for the spatial discretization of Eqs. (2.1) to (2.4) consist of P_p $(p \geq 2)$ Continuous Galerkin elements for the velocities and P_{p-1} Continuous Galerkin elements for the interfacial pressure. Thus, the interfacial pressure convergence order is lower than that for the velocity.

Taylor-Hood elements satisfy the Ladyzhenskaya-Babuška-Brezzi (LBB) condition, also known as inf-sup stability or div-stability condition (Mercier, 1979). The LBB condition is sufficient for saddle point problems with unique solutions that depend continuously on the input data.

The capability of the spatial discretization schemes to reproduce wave growth is investigated through the construction of eigenspectra for finite element schemes used for discretizing convection-dominated problems (i.e., Continuous Galerkin, Taylor-Hood, and MINI elements) (Alnæs et al., 2014).

Also, in this work, MINI elements are employed to compare the discretization schemes' effect on the eigenspectra for distinct scenarios. As stated in Arnold, Franco and Fortin (1984), enriching a finite element space can improve stability properties. MINI elements are composed of linear vector Continuous Galerkin elements enriched with a set of cubic vector Bubble elements and function space of continuous piecewise linear elements. The vector Bubble element is used for the velocity approximation (Logg; Mardal; Wells, 2012). For one-dimensional problems, the Bubble element B_q is defined for $q \geq (d+1)$.

The definition of the element space V_h depends on the element space, as follows:

- Continuous Galerkin: scalar-valued continuous p-order piecewise polynomials.
- Taylor-Hood: p-order scalar-valued continuous for the velocities, and $(p-1)$-order scalar-valued continuous piecewise polynomials for the liquid holdup and interfacial pressure.
- MINI: $p+1$-order enriched elements for the velocities and p-order scalar-valued continuous piecewise polynomials for the liquid holdup and interfacial pressure.

Equations 2.1 to 2.4 are resolved in horizontal and inclined pipelines, discretized in a uniform mesh. Horizontal, upward inclined pipes ($\beta = 0.25°$), and downward inclined pipes ($\beta = -5°$) are analyzed for instability and nonlinear studies (see Figs. 7a to 7c).

Figure 7 – Horizontal and slightly inclined straight pipes

(a) Horizontal

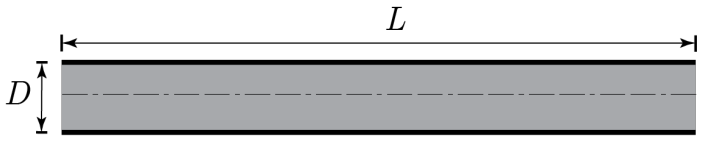

(b) Upward inclined

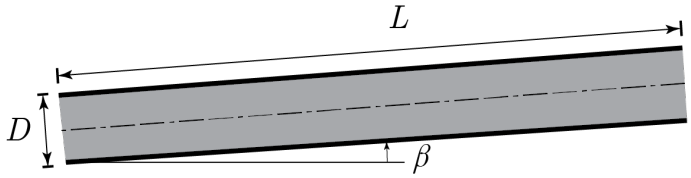

(c) Downward inclined

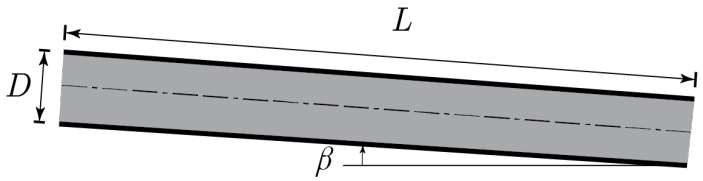

Note: adapted from Issa and Kempf (2003).

2.2.2 Time integration

The Two-fluid Model is regularly discretized through implicit time schemes (e.g., First-order Backward Differentiation Formula) because of its unconditional numerical stability. However, it is only first-order accurate and can introduce significant numerical diffusion (Sanderse; Smith; Hendrix, 2017). The Two-fluid Model equations are discretized with fully implicit time integration methods (see Table 2) according to the θ-method proposed in Barclay, Griffiths and Higham (2000).

Table 2 – Parameter values for time integration methods

Scheme	a_0	a_1	a_2	θ
BDF1	1	-1	0	1
BDF2	$\frac{3}{2}$	-2	$\frac{1}{2}$	1
CN	1	-1	0	$\frac{1}{2}$

Note: adapted from Sanderse, Smith and Hendrix (2017).

The left side of Eq. (2.24) can be written under the following expression (Smith, 2017; Sanderse; Smith; Hendrix, 2017):

$$\frac{a_0\mathbf{W}^{n+1} + a_1\mathbf{W}^{n} + a_2\mathbf{W}^{n-1}}{\Delta t} = \theta\mathbf{F}\left(\mathbf{W}^{n+1}, t^{n+1}\right) + (1-\theta)\,\mathbf{F}\left(\mathbf{W}^{n}, t^{n}\right) \tag{2.29}$$

with the parameter values given in Table 2. The local truncation for the methods is given by:

$$\bar{\tau}_{\text{CN, BDF}} = \left(\theta - \frac{1}{2}\right)\Delta t^2\mathbf{F}'' + \left(\frac{1}{2}\theta - \frac{1}{3}\right)\Delta t^3\mathbf{F}''' + \mathcal{O}\left(\Delta t^4\right) \tag{2.30}$$

The Courant–Friedrichs–Lewy (CFL) number (Courant; Friedrichs; Lewy, 1928; Courant; Friedrichs; Lewy, 2010) is taken as $C_{\text{CFL}} = 1$ as the first approach, based on the study of Sanderse, Smith and Hendrix (2017). However, for nonlinear simulations, the CFL numbers can be modified. Han and Guo (2015), stated that, in consideration of the stiffness of the problem, the time steps could be adjusted to ensure that the CFL numbers are less than **0.1** for all mesh cells. A variable time step is used for satisfying a CFL-type stability condition. The time step Δt is defined by:

$$\Delta t_k = \frac{C_{\text{CFL}} h_{\text{min}}}{\max\left|\lambda_n^{k-1}\right|} \tag{2.31}$$

where h_{min} is the minimum cell size of the mesh, $\max\left|\lambda_n^{k-1}\right|$ is the maximum characteristic at the previous time step, and C_{CFL} is a chosen positive number.

2.2.3 Initial and boundary conditions

As stated in Issa and Kempf (2003), Montini (2010), Bertodano et al. (2017), Zwieten et al. (2017), Ferrari, Bonzanini and Poesio (2017), the starting condition is a stratified smooth steady flow. Fig. 8 illustrates the layout of stratified smooth flow for horizontal and inclined straight pipes.

Figure 8 – Equilibrium stratified flow in inclined and horizontal pipes.

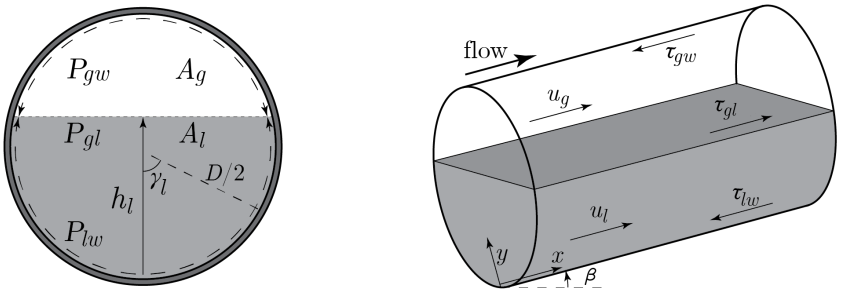

For stratified smooth flow, a momentum balance on each phase yields

$$\partial_{\mathbf{s}} p_i - \frac{\tau_{lw} S_{lw}}{A\alpha_l} + \frac{\tau_{gl} S_{gl}}{A\alpha_l} + \rho_l g \sin\beta = 0 \tag{2.32}$$

$$\partial_{\mathbf{s}} p_i - \frac{\tau_{gw} S_{gw}}{A\alpha_g} - \frac{\tau_{gl} S_{gl}}{A\alpha_g} + \rho_g g \sin\beta = 0 \tag{2.33}$$

Equating pressure drop in Eqs. (2.32) - (2.33) and assuming that the hydraulic gradient in the liquid is negligible gives

$$\tau_{gw}\frac{P_{gw}}{A_g} - \tau_{lw}\frac{P_{lw}}{A_l} + \tau_{gl} P_{gl}\left(\frac{1}{A_l} + \frac{1}{A_g}\right) + \left(\rho_g - \rho_l\right) g \sin\beta = 0 \tag{2.34}$$

where the shear stresses and geometric relations are evaluated as shown in Sections 2.1.2.1 and 2.1.2.2. The liquid fraction α_l^{eq} at the initial state can be calculated from Eq. (2.34) for given values of the superficial velocities. Equation (2.34) can be used for horizontal and slightly inclined pipes (Issa; Kempf, 2003; Holmås et al., 2008; Liao; Mei; Klausner, 2008; Bonzanini; Picchi; Poesio, 2017; Sanderse; Smith; Hendrix, 2017; Hendrix et al., 2016).

Three boundary conditions must be set at the inlet and one at the outlet:

1. Liquid volumetric fraction: $\alpha_l\left(s=0,t\right) = \alpha_l^{in}$,
2. Superficial liquid velocity: $u_l\left(s=0,t\right) = u_l^{in}$,
3. Superficial gas velocity: $u_g\left(s=0,t\right) = u_g^{in}$,
4. Absolute interfacial pressure: $p_i\left(s=L,t\right) = p_i^{out}$.

2.3 Stability

The stability regions for different initial conditions are determined by analyzing Kelvin-Helmhotz-type instabilities. According to (Barnea; Taitel, 1994), the curves representing the limit of well-posedness coincide with the Inviscid Kelvin Helmholtz (IKH) limit. Among other authors, Barnea and Taitel (1994) studied the effect of liquid viscosity on stability. They concluded that the neutral stability curves coincide with the Viscous Kelvin-Helmholtz (VKH) limit and approximate the transition from stratified to intermittent flow in horizontal pipes. In

contrast, Bendiksen and Espedal (1992) argued that the VKH does not provide necessary and sufficient conditions for the onset of slugging and only gives the transition from stratified smooth to stratified wavy flow.

2.3.1 Well-posedness analysis

The well-posedness criteria reveal the hyperbolicity of the model through its characteristics (Fletcher, 2012; Hirsch, 1988b; LeVeque, 2002; Montini, 2010). A problem is well-posed when the solution exists, is unique, and depends continuously on the initial data (Hadamard, 1902). When these conditions are satisfied, the problem is well-posed, and any perturbation can grow as it propagates along the domain. As stated in Issa and Kempf (2003), Montini (2010), the ill-posedness character of the Two-fluid Model is not influenced by the energy equations. Substituting wave-like solutions (Hirsch, 1988a; Drew; Passman, 1998; Sanderse; Smith; Hendrix, 2017) in the homogeneous part of (2.7):

$$\mathbf{W} = \widehat{\mathbf{W}} e^{i(n_s s + n_t t)} \tag{2.35}$$

letting $\lambda_n = -n_s/n_t$, the generalized eigenvalue problem reads:

$$\det(\mathbf{B} - \lambda_n \mathbf{A}) = 0 \tag{2.36}$$

Equation (2.36) has n eigenvalues λ_n for the n equations, which represent the velocities and their eigenvectors, the direction of propagation of the information (Sanderse; Smith; Hendrix, 2017). Based on the characteristics, according to Montini (2010);

- If Im$(\lambda_n) = 0$ the equation system is parabolic and well-posed;
- If Im$(\lambda_n) = 0$, and λ_n are different the equation system is hyperbolic and well-posed;
- If Im$(\lambda_n) \neq 0$ the equation system is elliptic and ill-posed.

2.3.2 Fourier analysis

The Fourier analysis studies the response of the linearized equations when imposing infinitesimal perturbations (i.e., solitary waves on the interface (Pokharna; Mori; Ransom, 1997; Ansari, 1998)). The information on the growth rate of the instabilities around equilibrium solutions (Ramshaw; Trapp, 1978) is provided through a Fourier analysis, concordantly with Liao, Mei and Klausner (2008), Montini (2010), Fullmer (2014).

Equations (2.1) - (2.4) are linearized around a reference state with an infinitesimally small perturbation $\mathbf{W} = \mathbf{W}_0 + \widetilde{\mathbf{W}}$ imposed. The linearized equations read:

$$\mathbf{A}_0(\mathbf{W}_0)\partial_t \widetilde{\mathbf{W}} + \mathbf{B}_0(\mathbf{W}_0)\partial_{\mathbf{s}} \widetilde{\mathbf{W}} + (\partial_W \mathbf{C})_0(\mathbf{W}_0)\widetilde{\mathbf{W}} = 0 \tag{2.37}$$

where $\mathbf{A}_0$, $\mathbf{B}_0$ and $(\partial_W \mathbf{C})_0$ are evaluated at the reference state $\mathbf{W}_0$. The linearization process of the Two-fluid Model is presented in Appendix 4.2.

The perturbation is assumed to be of a wave-like form $\varepsilon e^{[I(\omega t - ks)]}$ with amplitude ε, angular frequency ω and wavenumber k, leading to:

$$\left(\mathbf{A}_0\left(\mathrm{I}\omega\right) - \mathbf{B}_0\left(\mathrm{I}k\right) + \left(\partial_W \mathbf{C}\right)_0\right)\varepsilon e^{\mathrm{I}(\omega t - ks)} = 0 \tag{2.38}$$

where the imaginary component $\mathrm{Im}(\omega)$ of the angular frequency represents the wave growth rate. Equation (2.38) has a non-trivial solution if the determinant of the coefficient matrix vanishes:

$$\det\left(\mathbf{A}_0\left(\mathrm{I}\omega\right) - \mathbf{B}_0\left(\mathrm{I}k\right) + \left(\partial_W \mathbf{C}\right)_0\right) = 0 \tag{2.39}$$

The Two-fluid Model leads to a nonlinear dispersive system of equations (i.e., waves of different wavelengths propagate at different phase velocities (Dodd et al., 1982; Montini, 2010)). The variation of the wave growth rate of the disturbances with the wavenumber is studied through the resolution of Eq. (2.39).

For a single wave with $k = 2\pi$ (i.e., the smallest wave number presented on the domain), the dispersion equation (2.39) can be solved for the wave frequency. The solution leads to 4 waves, two convective and two acoustic waves. Fullmer et al. (2010), Pokharna, Mori and Ransom (1997), VonNeumann and Richtmyer (1950) affirmed that the Fourier analysis provides a stability condition of the equation system based on the growth rate of disturbances $-\mathrm{Im}(\omega_n)$ for distinct wavelengths.

- If $-\mathrm{Im}(\omega_n) < 0$ the system is stable and the flow is stratified smooth,
- If $-\mathrm{Im}(\omega_n) = 0$ the system is neutrally stable;
- If $-\mathrm{Im}(\omega_n) > 0$, the system is unstable, leading to stratified wavy flow and the eventual flow pattern transition to intermittent flow;
- If $-\mathrm{Im}(\omega_n)$ exponentially blows up for short wavelengths λ and the equation system is ill-posed.

2.3.3 Stiffness analysis of the semi-discrete equations

The Fourier analysis of the differential equations (see Section 2.3.2) studies the stability of the equation system at the initial conditions. Ultimately, Eqs. (2.1) - (2.4) are discretized in space (see Equation 2.24). Some terms in the differential equations lead to fast transients, while others are slow (Sanderse; Smith; Hendrix, 2017), which makes the semi-discrete equations (2.24) stiff. The stiffness is studied through eigenvalue analysis of the semi-discrete equations. The eigenspectrum reveals the feasibility of the spatial discretization scheme for capturing instabilities or reproducing wave growth. It depends on several factors, including the grid size, the order of the basis functions, gas compressibility, and grid size.

Equations (2.1) - (2.4) are semi-discretized, leading to a semi-discrete system, only depending on time, following the procedure of (Sanderse; Smith; Hendrix, 2017), reading:

$$\frac{d\mathbf{U}}{dt} = \mathbf{F}(\mathbf{U}), \tag{2.40}$$

where $\mathbf{U} = \mathbf{U}(t) \in \mathbb{R}^{qN}$ is the vector of conserved variables:

$$\mathbf{U} = \left[\left(\alpha_l \rho_l \right), \left(\alpha_g \rho_g \right), \left(\alpha_l \rho_l u_l \right), \left(\alpha_l \rho_l u_l \right) \right]^T \tag{2.41}$$

Equation (2.41) is linearized around the initial condition (see Section 2.2.3): $\mathbf{W} = \mathbf{W}_0 + \widetilde{\mathbf{W}}(t)$. The semi-discrete system only depends on time. It can be written as:

$$\frac{d\mathbf{W}}{dt} = \mathbf{J}\widetilde{\mathbf{W}} \tag{2.42}$$

where $\mathbf{J} = (\partial_{\mathbf{W}}\mathbf{F}) \in \mathbb{R}^{qNxqN}$. Diagonalization of $\mathbf{J} = \mathbf{K}\mathbf{D}\mathbf{K}^{-1}$ leads to the following set of decoupled equations:

$$\frac{d\widetilde{\mathbf{Z}}}{dt} = \mathbf{D}\widetilde{\mathbf{Z}} \tag{2.43}$$

where $\mathbf{Z} = \mathbf{K}^{-1}\mathbf{U}$. The matrix $\mathbf{D}$ is a diagonal matrix with eigenvalues ω_N of $\mathbf{J}$. These eigenvalues are the discrete approximation of the eigenvalues of only the spatial derivatives of the Two-fluid Model.

2.3.4 Wave growth prediction through von Neumann analysis

For unstable initial conditions, infinitesimal disturbances imposed on the equilibrium state grow with different growth rates for each time step and position in the pipe, presenting the possibility of the emergence of waves, which can grow until blocking the pipe diameter, producing intermittent flow, or they can be attenuated due to gravity, viscous forces, the configuration of the pipeline or the numerical diffusion of the numerical method (Taitel; Dukler, 1976; Issa; Kempf, 2003; Montini, 2010).

Differential flow pattern maps display stable and unstable regions based on the Kelvin-Helmholtz stability theory (Taitel; Dukler, 1976). Experimental flow pattern maps show transition curves and flow pattern regions in steady-state. Ultimately, discrete flow pattern maps introduced in Sanderse, Smith and Hendrix (2017) display the effective stability regions when the discrete equations are solved with a particular numerical method, grid, and time resolution.

The Discrete Flow Pattern Maps are constructed through the von Neumann analysis (VonNeumann; Richtmyer, 1950) and indicate whether a discretization method can correctly capture the unstable well-posed regime and the potential transition to slug flow or if numerical diffusion overwhelms the physical growth of instabilities. During transient simulations, growth rates can differ from those obtained from the dispersion analysis of the differential equations because of the numerical diffusion involved in some schemes (Sanderse; Smith; Hendrix, 2017).

The spatial discretization eigenvalues should fall inside the stability region for the time integration method, which is constructed by application of the time integration method described by Eq. (2.29) to a linear test equation (as derived from Eq. (2.43)) following the

procedure of Sanderse, Smith and Hendrix (2017):

$$\dot{v}(t) = \omega v dt, \omega \in \mathbb{C} \tag{2.44}$$

The application of the time integration method (see Eq. (2.29)) to Eqs. (2.1) - (2.4) leads to the following equation for the numerical growth rate (i.e., amplification factor) G:

$$\left(a_0 - \omega \Delta t \theta\right) G^2 + \left(a_1 - \omega \Delta t \left(1 - \theta\right)\right) G + a_2 = 0 \tag{2.45}$$

where the coefficients a_0, a_1, and a_2 are defined in Table 2 The amplification factor G indicates whether the numerical solution will grow in time, and is defined by:

$$G(z) = \left| \frac{v^{n+1}}{v^n} \right| \tag{2.46}$$

where $z = \omega_N \Delta t$.

2.4 Regularization of the Two-fluid Model

Since the Two-fluid model equations represent a dispersive system, and wavelengths shorter than a cut-off value λ_0 can be considered insignificant (see Section 1.2), it is desirable to have an energy sink in the numerical scheme at a short wavelength (i.e., $\lambda \approx 2\Delta x$) to keep these wavelengths from growing and affecting the solution. The numerical scheme amplification factor for $\lambda = 2\Delta x$ should be less than one. However, in some cases, it does not resolve the fundamental ill-posed behavior of the Two-fluid Model in a physical sense, and it may preclude convergence beyond the IKH criterion.

Second-order numerical diffusion terms can be added to all equations to achieve a cut-off wavenumber beyond which perturbations decay. Montini (2010) added axial diffusion terms in the momentum equations. They used Fick's law of diffusion (i.e., $J = -\nabla \Gamma \phi$ (Fick, 1855), where J is the diffusion flux, Γ is the diffusion coefficient, and ϕ is a generic concentration). Bonzanini, Picchi and Poesio (2017), Holmås et al. (2008), Montini (2010) introduced ad-hoc diffusion-like terms into the Two-fluid Model equations and solved the Two-fluid Model in horizontal pipes. Appendix 4.2 presents a regularized Two-fluid Model equation system with numerical diffusion.

As a first approach, ad hoc numerical diffusion can be added to the equation system to study the capability of the numerical model to describe the effect of the wavelength on the growth rate of disturbances. The gas and liquid coefficients are considered equal for the mass and momentum diffusion (i.e., $\Gamma_l = \Gamma_g = \Gamma$ and $\nu_l = \nu_g = \nu$).

2.5 Implementation

The numerical model is written in the Python 3 programming language (with a few C++ extensions) (Rossum; Drake, 2009) with the aid of the open-source computing FEniCS

Project platform (Alnæs et al., 2015; Logg; Mardal; Wells, 2012). After formulating the variational problem, the FEniCS framework is used to construct the basis functions, solve the integral functions on the element level, and assemble the system matrix.

For the stability analysis (see Section 2.3.2), the linearization of the Two-fluid Model is performed with Wolfram Mathematica (Wolfram Research, Inc., 2020). The solution to the equation system (2.34) at the initial state is solved through the secant method. The solution to generalized eigenvalue problems of Sections 2.3.1, 2.3.2, and 2.3.3 is accomplished with the Python 3 language through the ARPACK library (Lehoucq; Sorensen; Yang, 1998).

In the well-posedness analysis, equation (2.36) is resolved through the Arnoldi Package (ARPACK) library (Lehoucq; Sorensen; Yang, 1998), and the Portable, Extensible Toolkit for Scientific Computation (PETSc) suite (Balay et al., 2019; Katz et al., 2007). In the Fourier analysis, equation (2.39) is numerically solved with ARPACK functions, which use the Implicitly Restarted Arnoldi Method (Lehoucq; Sorensen; Yang, 1998, 1998) to find the angular frequencies.

The Jacobian is obtained using the symbolic differentiation of FEniCS for nonlinear simulations through the Newton linearization method. The linear system is solved through the Unsymmetric MultiFrontal method (UMFPACK) method (Davis, 2004; Duff; Scott, 2004) available in the Portable, Extensible Toolkit for Scientific Computation (PETSc) suite (Balay et al., 2019; Katz et al., 2007).

3 RESULTS AND DISCUSSION

This chapter presents the results and the discussion through sensitivity studies on the capability of the numerical model to reproduce wave growth. Furthermore, differential and hybrid flow pattern maps (i.e., a combination of differential, discrete, and experimental) show the regions where flow pattern transitions may occur. The numerical model is also validated through data available in the literature.

This work resulted in two oral presentations in conferences (Lazo-Vásquez; Baliño, 2022; Lazo-Vásquez; Baliño, 2023a) (see the conference papers in Annexes 4.2 and 4.2), a journal paper submission (see Annex 4.2), and a co-authorship of a conference paper about a unit-cell approach for predicting slug flow in steady-state (Pellegrini et al., 2019) (see the conference paper in Annex 4.2). The Model implementation is available online in a GitHub repository (Lazo-Vásquez; Baliño, 2023b).

The numerical model proposed in this thesis (Lazo-Vásquez; Baliño, 2023b) has the capability of performing: stability analysis of the linearized equations, stiffness analysis of the semi-discrete equations, transient simulations of the fully-discrete equations, and the construction of hybrid flow pattern maps. The inputs (i.e., phase properties, the geometry of the pipes, and flow conditions) and outputs of the model are shown in Fig. 9:

Figure 9 – Inputs and outputs of the model

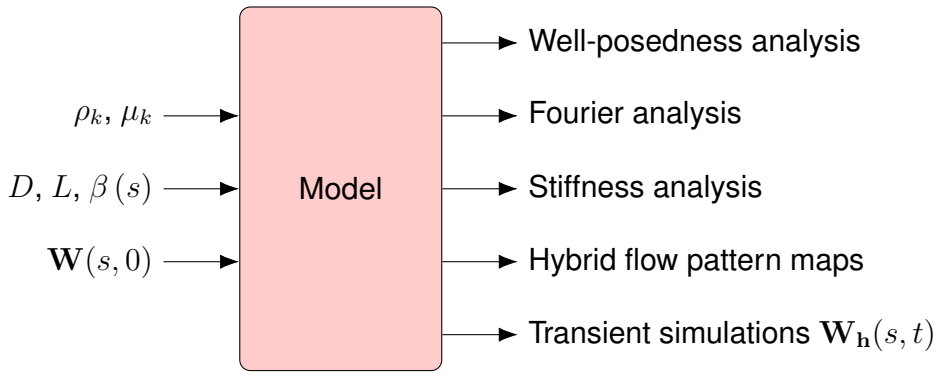

Note: the subscript $k \in \{l, g\}$, $\mathbf{W} = [\alpha_l, u_l, u_g, p]^\mathsf{T}$, s is the spatial coordinate, and t is the time coordinate.

The equation system to be resolved by the model can be set as an input or selected from a list, consisting of the two-fluid model equations in the primitive and conservative forms. The code allows the addition of other equation systems, being convection-dominated or not, enabling studies on finite-element spaces, time discretization schemes, and other simulation parameters.

The results are organized as follows. First, a well-posedness and Fourier analyses of the differential equations show the regions where the two-fluid model equations can be resolved at the initial conditions. The eigenspectra at different initial conditions reveal the characteristics and modes associated with such regions. Also, through a dispersion analysis, for diverse initial conditions, the dispersive behavior of the equation system is investigated,

showing the relationship between wavelengths and stability. As an example, the capability of the model for regularization studies is presented by adding numerical diffusion to damp short wavelengths associated with ill-posedness. The model uses *ad-hoc* coefficients.

Second, considering stratified smooth flow at the initial conditions, after spatially discretizing the Two-fluid Model equations, a stiffness analysis is performed aiming to reveal the influence of different finite element formulations on stability. Also, the modes of the eigenspectra are analyzed through the variation of some parameters, including pipe inclination, number of elements, and order of the basis functions.

Third, after discretizing the two-fluid model equations with implicit time schemes, fully discrete flow pattern maps are constructed through transient simulations during the first time steps, revealing the factual stability of the equations in time. Finally, through a combination of well-posedness and neutral stability curves, hybrid flow pattern maps for different pipe inclinations serve to analyze the possible discrepancies between the differential and numerical solutions and the necessity of the inclusion of terms in the equations.

3.1 Initial conditions and parameters

In the numerical simulations and stability studies, the phase properties adopted are the same as Issa and Kempf (2003), Montini (2010), Sanderse, Smith and Hendrix (2017) to ease validation of the results. The geometry is determined by the correlations described in Section 2.1.2.1 for straight pipes (see Fig. 7). The initial conditions, i.e., $\mathbf{W}(s,0)$, are obtained through the characterization of air-water stratified smooth flow (see Eqs. 2.34). The liquid phase density is considered constant, and the gas phase is compressible. The fluid properties and other parameter values that remain constant in this study are shown in Table 3.

Table 3 – Parameter values that remain constant.

Parameter	Value	SI unit
ρ_l	1000	$kg\ m^{-3}$
$p_{i,0}$	10^5	Pa
c_g	343	$m\ s^{-1}$
L	1	m
g	9.8	$m\ s^{-2}$
μ_l	$1.8 \cdot 10^{-5}$	$Pa\ s$
μ_g	$8.9 \cdot 10^{-4}$	Pa s

The phenomenological flow pattern maps of Shoham (1982), Barnea and Taitel (1994), validated with experimental data of steady-state air-water flow, served as the theoretical transition boundaries. Table 4 shows the parameters of the experimental flow pattern maps employed to validate differential and numerical flow pattern maps.

Table 4 – Test cases for validating differential flow pattern maps with experimental data.

Case	β [deg]	D [cm]	Validation
Ia	0	5.1	Shoham (1982), Barnea and Taitel (1994)
Ib	0.25	5.1	Shoham (1982), Barnea and Taitel (1994)
Ic	-5	5.1	Shoham (1982), Barnea and Taitel (1994)
Id	0	7.8	Sanderse, Smith and Hendrix (2017)

3.2 Stability at the initial conditions

3.2.1 Well-posedness analysis

The well-posedness analysis (Section 2.3.1) reveals the regions where the Two-fluid Model keeps its hyperbolicity. Above the limits of well-posedness, the equation system should be regularized to be solved with any standard numerical method. The curves representing the limit of well-posedness are built with a sequence of superficial velocities. The computations are stopped when complex eigenvalues are found, i.e., the equation system is no longer hyperbolic. Four eigenvalues associated with the characteristics are obtained. Two of them ($\lambda_{1,2} \approx \pm c$) are related to the speed of sound c, and the others ($\lambda_3 \approx u_{sl}$, and $\lambda_4 \approx u_{sg}$) are related to the speed of the convective waves (Wallis; Wallis, 1969).

The limits of well-posedness can coincide with the IKH criteria for horizontal and slightly inclined pipes (see Section 2.3.1). Figure 10 shows the influence of local pipe inclination on the limits of well-posedness. In upward inclined pipes, the limits of well-posedness of the Two-fluid Model limits arise at lower liquid superficial velocities, which implies the need for regularization at higher flow rates. Table 5 presents the test points used as initial conditions in well-posed analysis and further stability studies.

Table 5 – Test points for differential flow pattern maps

Test point	u_{sl} $[m/s]$	u_{sg} $[m/s]$
□	0.05	0.829
◯	0.5	6.908
△	0.7	10.0

Note: data from Sanderse, Smith and Hendrix (2017).

Figures 12b and 11 depict the influence of the local inclination of the pipeline on the characteristics. When the model becomes ill-posed, complex eigenvalues arise. The system is well-posed for all the initial conditions studied in downward inclined pipes (see Fig. 11). Alternatively, in upward inclined pipes, ill-posedness arises at lower liquid superficial velocities.

Figure 10 – Effect of local inclination on the limit of well-posedness for horizontal and inclined pipes with $D = 0.078\ m$.

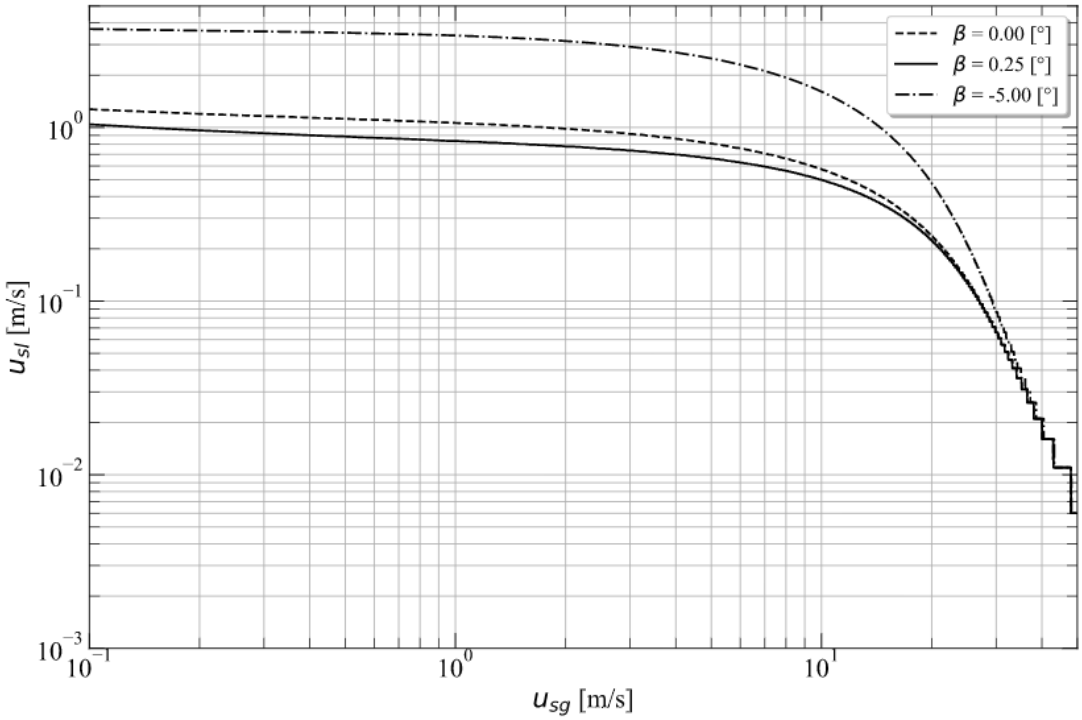

Figure 11 – Effect of flow conditions and local inclination on the characteristics of the differential equation system $D = 0.078\ m$.

(a) Downward inclined pipe ($\beta = -5\ deg$).

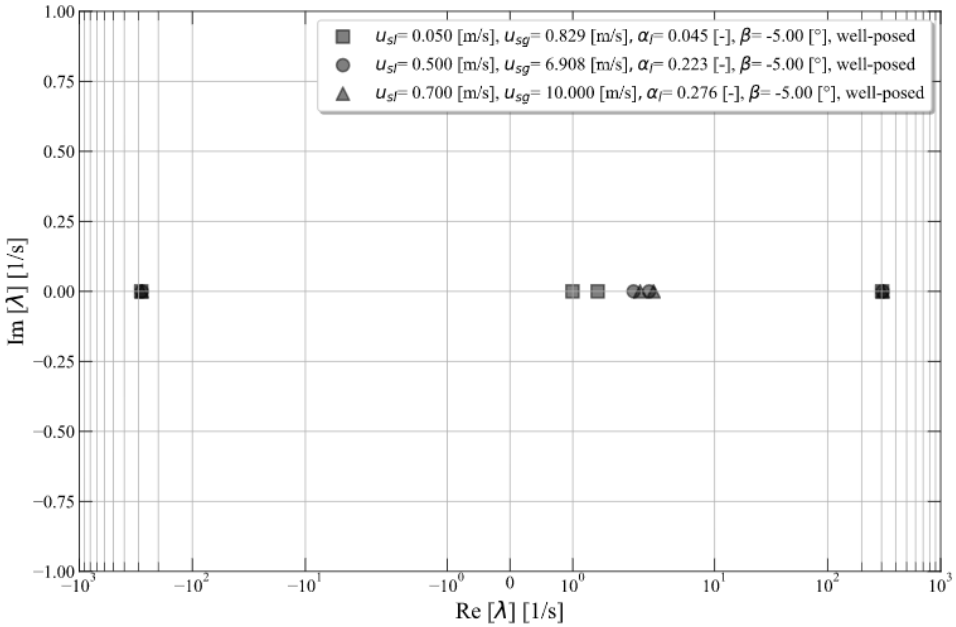

Figure 12 – Effect of flow conditions and local inclination on the characteristics of the differential equation system ($D = 0.078\ m$).

(a) Horizontal pipe ($\beta = 0\ deg$).

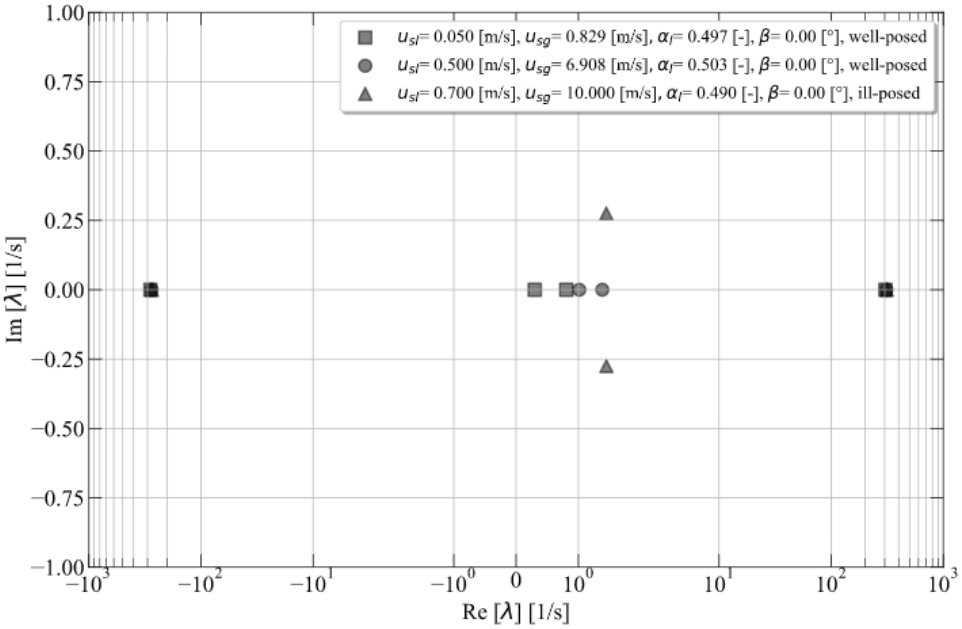

(b) Upward inclined pipe ($\beta = 0.25\ deg$).

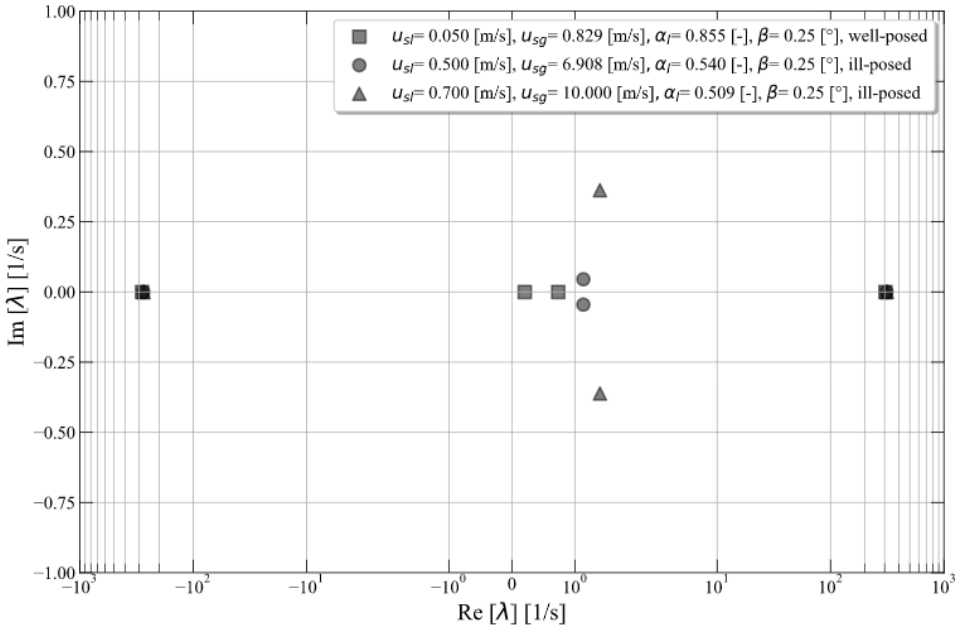

3.2.2 Fourier analysis

The dispersion relation (2.39) indicates how waves with distinct wavelengths can lead to different growth rates of disturbances. The growth rate of disturbances varies due to the dispersive character of the equation system, which is shown in Fig 13, which details the effect of the wavelength λ on the complex angular frequencies ω. The wave-growth rate is always finite for well-posed initial conditions for any wavelength. However, such growth rates

can be infinite for ill-posed cases for short wavelengths. Alternately, Fig 14 shows the effect of a regularized equation system according to Section 2.4.

Figure 13 – Effect of initial conditions on the dispersion of a non-regularized model

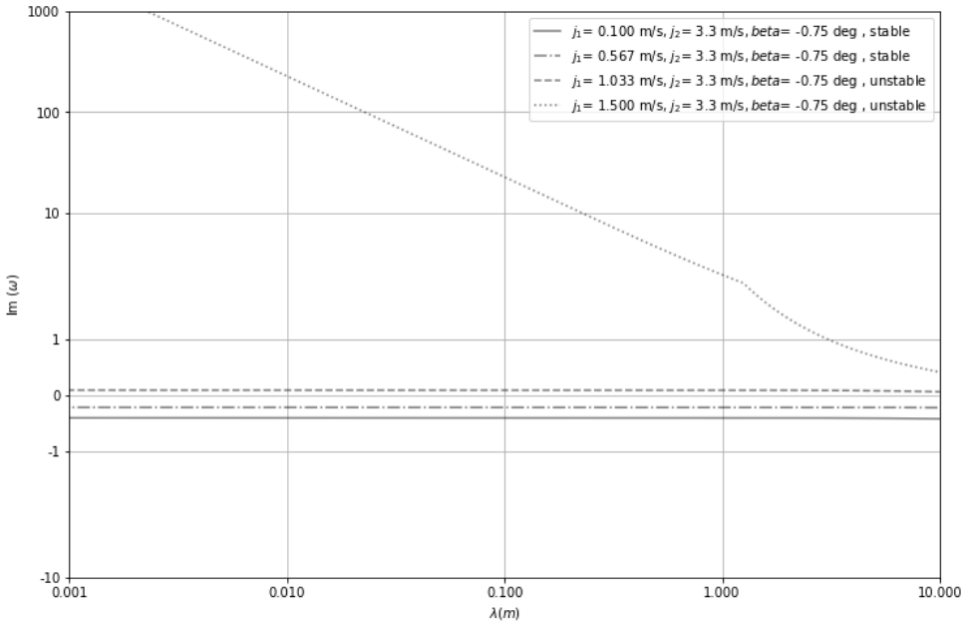

The parameters j_l and j_g stand for the liquid and gas superficial velocities

Figure 14 – Effect of initial conditions on the dispersion of a regularized model

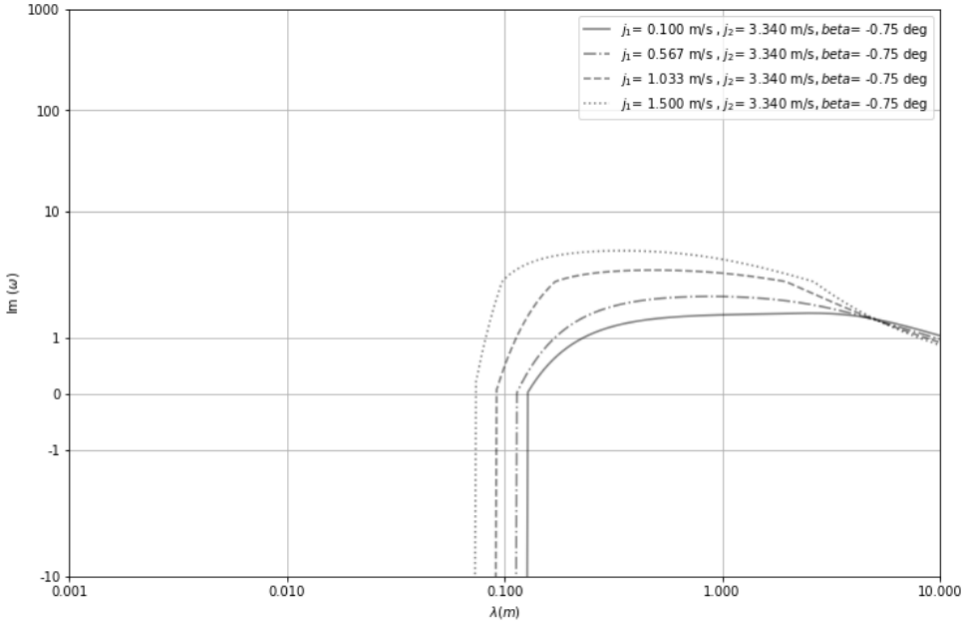

The parameters j_l and j_g stand for the liquid and gas superficial velocities

For a single wave with $k = 2\pi$, the dispersion relation (see Eq. (2.39) led to an eigenvalue problem, which is solved for a sequence of superficial velocities. When positive complex angular frequencies are found, the system is considered stable; alternatively, when negative

complex angular frequencies are found, the system is unstable. When real angular frequencies appear, the system is neutrally stable. The eigenspectra shown in Fig. 17 provide information about the initial conditions. The system leads to two convective waves and two acoustic waves. Three of them travel forward, and the last one backward. That is why one boundary condition is chosen at the pipe outlet. In transient simulations, traveling waves based on the data of the eigenspectra can be imposed as initial perturbations (Sanderse; Smith; Hendrix, 2017), forcing the emergence of waves.

Figure 15 – Effect of the local inclination on the eigenspectra for $D = 0.078\ m$.

(a) Horizontal pipe ($\beta = 0\ deg$).

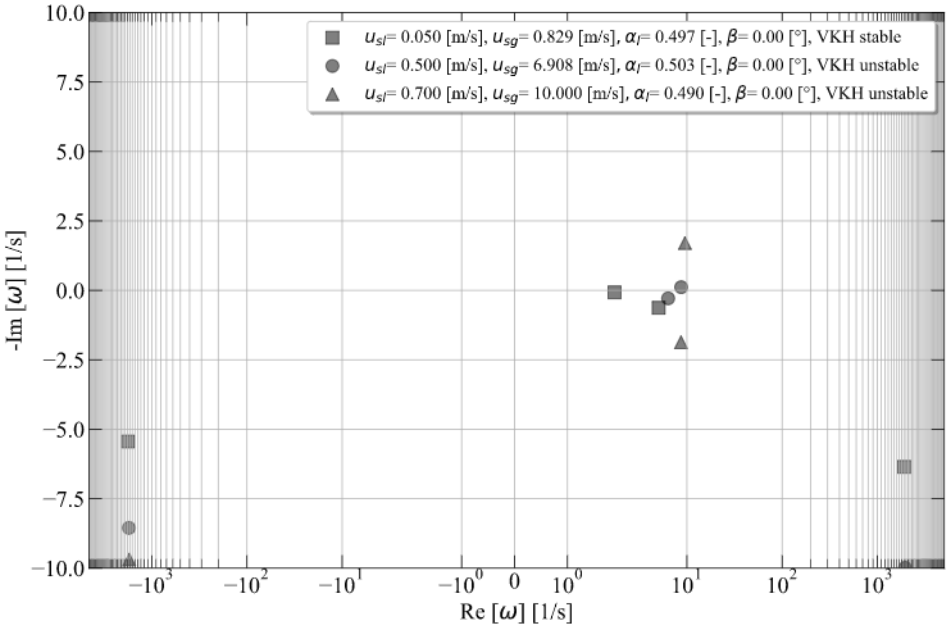

Figure 16 – Effect of the local inclination on the eigenspectra for $D = 0.078\ m$.

(a) Upward inclinedpipe ($\beta = 0.25\ deg$).

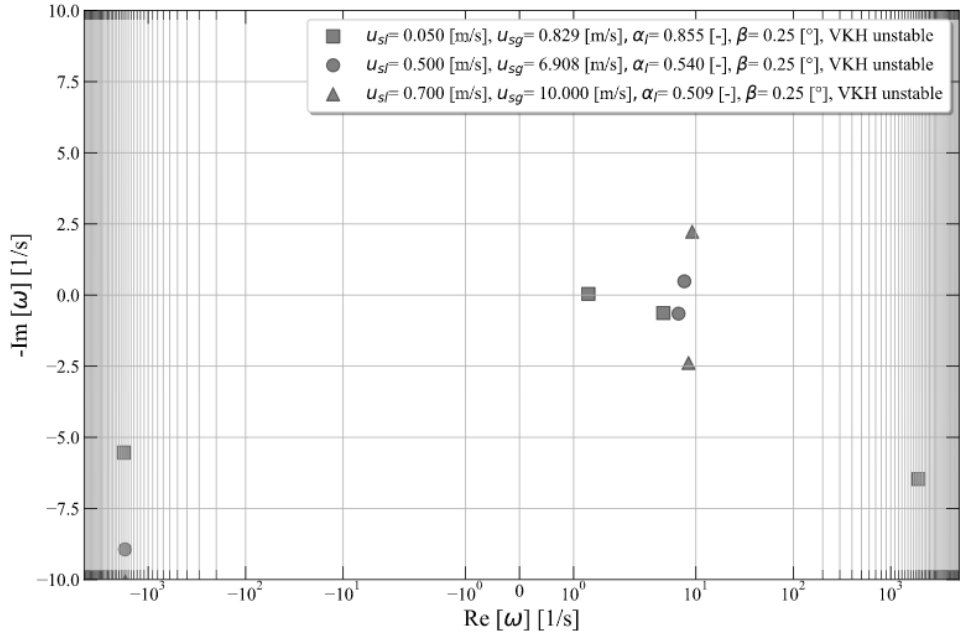

Figure 17 – Effect of the local inclination on the eigenspectra for $D = 0.078\ m$.

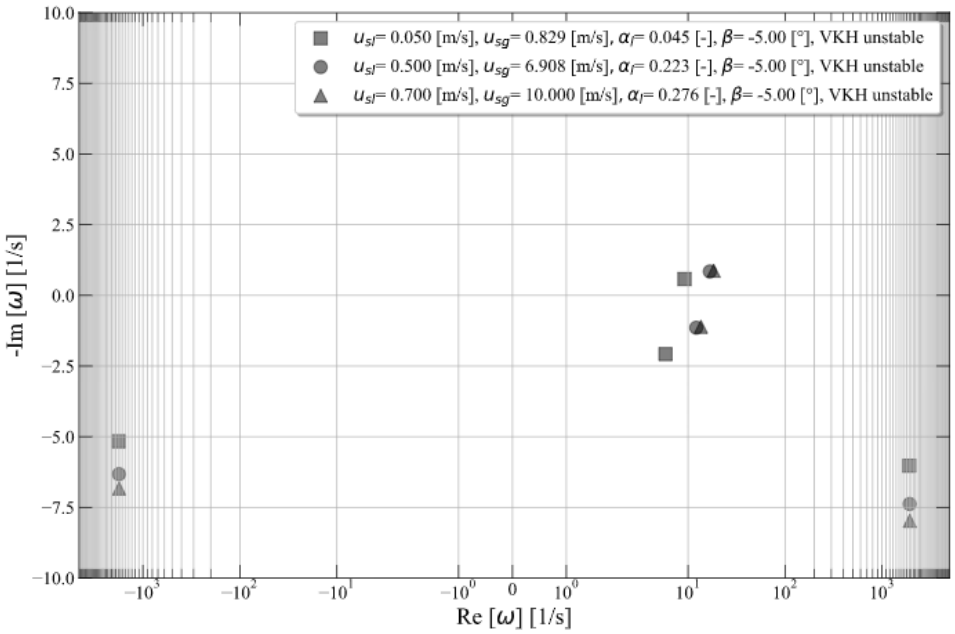

(a) Downward inclinedpipe ($\beta = 0\ deg$).

3.3 Stiffness analysis of the semi-discrete equations

The eigenspectra of the semi-discrete equations are related to the capability of the spatial discretization schemes to reproduce wave growth. Table 6 reports the test cases for sensitivity studies on the Effect of the mesh size, the order of basis functions, superficial velocities, the local inclination of the pipeline, and the type of element spaces on the stiffness of the equations.

Figure 18 illustrates the effect of the finite-element space on the stiffness of the problem. The eigenmodes corresponding to convective waves have the largest real components for unstable initial conditions. Conversely, the eigenmodes corresponding to acoustic waves have the largest imaginary components. Convective waves may lead to instabilities in the Two-fluid Model semi-discretized equations when associated with positive real eigenmodes.

The structure of the eigenspectra is preserved in Case I, which suggests that the methods can reproduce wave growth. The following sensitivity studies are performed with higher-order Taylor-Hood elements, known for preserving the inf-sup condition. Moreover, MINI elements are known for their improved stability, which can be beneficial during transient simulations and the prediction of flow pattern transitions.

Table 6 – Test cases for stiffness analysis of the semi-discrete Two-fluid Model

Sensitivity analysis	Elements	Case	N	q	$u_{sl}\ [m/s]$	$u_{sg}\ [m/s]$	$\beta\ [deg]$
Element space	CG	Ia	40	2	0.50	6.908	0
	TH	Ib	40	2	0.50	6.908	0
	MINI	Ic	40	2	0.50	6.908	0
Local inclination	TH	IIa	40	2	0.50	6.908	0
	TH	IIb	40	2	0.50	6.908	0.25
	TH	IIc	40	2	0.50	6.908	-5
Number of elements	TH	IIIa	40	2	0.50	6.908	0
	TH	IIIb	80	2	0.50	6.908	0
	TH	IIIc	160	2	0.50	6.908	0
Order of basis functions	TH	IVa	40	2	0.50	6.908	0
	TH	IVb	40	4	0.50	6.908	0
	TH	IVc	40	6	0.50	6.908	0
Superficial velocities	TH	Va	40	2	0.05	0.829	0
	TH	Vb	40	2	0.50	6.908	0
	TH	Vc	40	2	0.70	10.000	0

Note: the acronyms CG and TH stand for Continuous Galerkin and Taylor-Hood, respectively. The acronym MINI stands for linear vector Continuous Galerkin elements enriched with a set of cubic vector Bubble elements.

Figure 18 – Effect of discretization of convective and source terms with distinct finite-element spaces on the stiffness (case I).

(a) Continuous Galerkin elements $\mathcal{P}_2$.

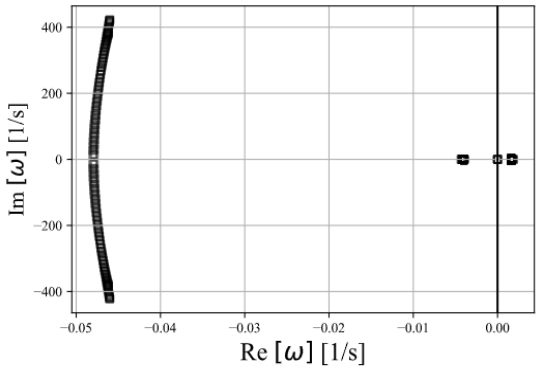

(b) Taylor-Hood elements $\mathcal{P}_2 - \mathcal{P}_1$.

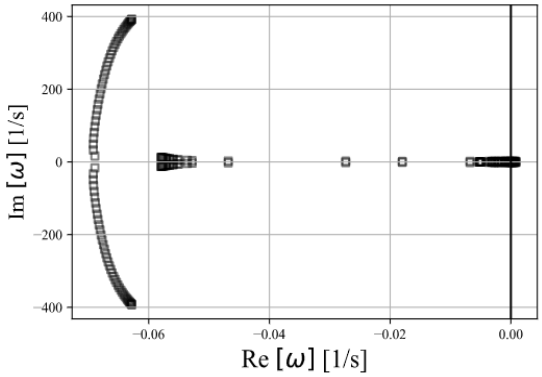

(c) MINI elements $\mathcal{P}_1 - \mathcal{B}_3$.

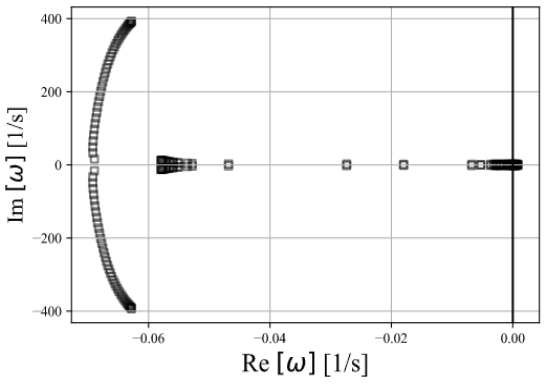

Figures 19 to 22 show the spectrum of the Two-fluid Model semi-discrete equations for

the parameter values of table 6 with Taylor-Hood element spaces. As shown in Fig 19, they can have real positive components for different initial conditions. There are no real positive modes for well-posed stable initial conditions; otherwise, they have positive real modes. Therefore, convective waves may produce wave growth without being attenuated.

Figure 19 – Effect of the superficial velocities on the stiffness (case II)

(a) Well-posed stable (case IIa)

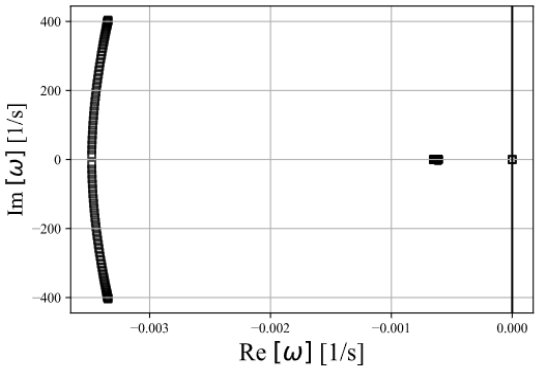

(b) Well-posed unstable (case IIb).

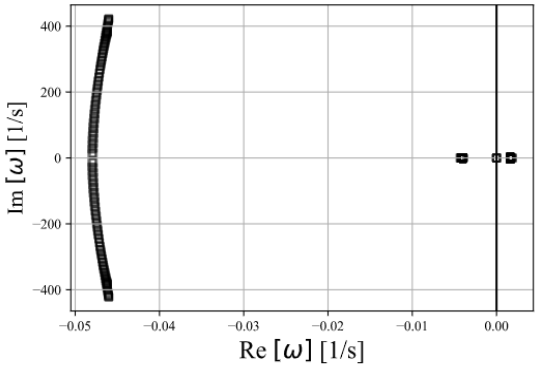

Note: spatial discretization of the convective and source terms with Continuous Galerkin P_2 elements.

Figure 20 – Effect of the local inclination on the stiffness (case II:). Spatial discretization of the convective and source terms with Continuous Galerkin P_2 elements.

(a) Horizontal pipe ($\beta = 0\ deg$) (case IIIa).

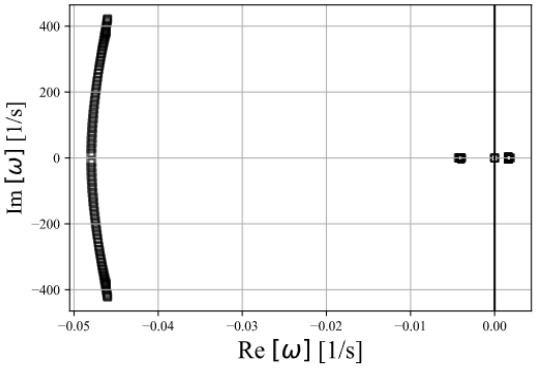

(b) Upward inclinedpipe ($\beta = 0.5\ deg$) (case IIIb).

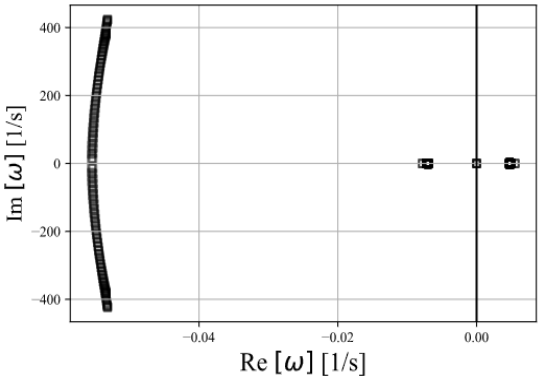

(c) Downward inclinedpipe ($\beta = -1.5\ deg$) (case IIIc).

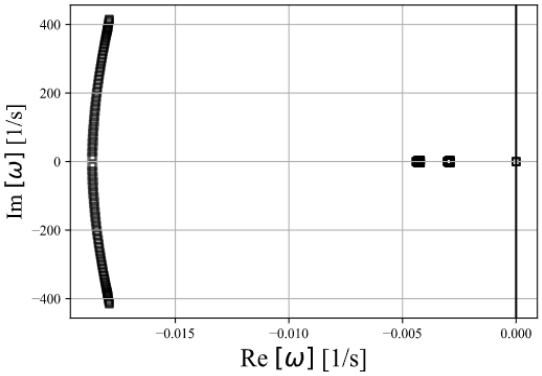

Figure 20 shows the pipe local inclination's influence on the waves' emergence. For downward inclined pipes with $\beta = -1.5°$ (see Fig. 20c), they are just a few real positive

modes with a low growth rate of disturbances, which suggests that it is not feasible to develop waves with higher growth rates. However, for horizontal and upward inclined pipes, the real positive part of the modes has disturbances with a higher growth rate, validating the differential flow pattern maps.

With an unstable well-posed initial state, Fig. 21 shows the influence of the mesh size. Notably, for a horizontal mesh of 400 elements, there is a larger number of modes; however, the disposition of the spectrum does not change. It is still possible to reproduce wave growth. Fig 21 shows the structure of the eigenspectrum changes for incompressible flow. The figure depicts eigenmodes in both negative and positive real parts. The largest imaginary components of the modes reduce to 100, and the modes representing acoustic waves are displaced near the origin.

Figure 21 – Case IV: Effect of mesh size on the stiffness. Spatial discretization of the convective and source terms with Continuous Galerkin P_2 elements.

(a) Coarse mesh ($N = 40$) (Case IVa) (b) Fine mesh ($N = 400$) (case IVb).

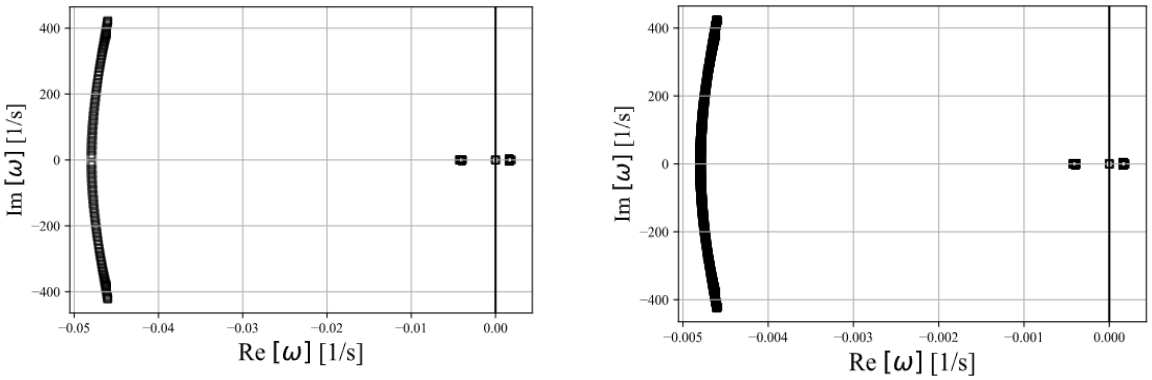

Figure 22 – Effect of the order of basis functions on the stiffness (case IV).

(a) Low-order basis functions $(k = 2)$ (case IVa). (b) Higher-order basis functions $(k = 6)$ (case IVb).

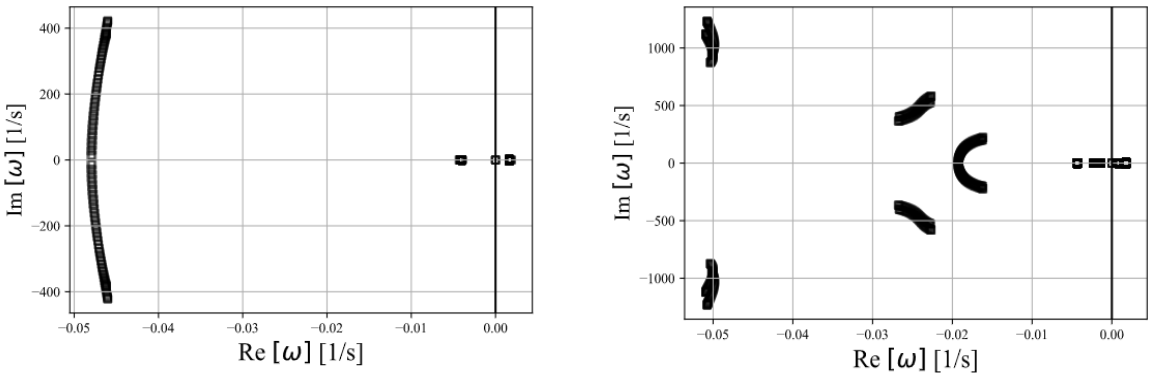

Figure 22 depicts the influence of the order of the basis functions. For higher-order basis functions, the eigenspectra change; however, it is possible to simulate wave growth. The eigenmodes corresponding to acoustic waves acquire higher maximum rates and structure changes. However, the structure of the eigenmodes corresponding to the convective waves is maintained, having higher real positive values.

3.4 Flow pattern prediction based on Kelvin-Helmholtz instabilities

3.4.1 Differential flow pattern maps at the initial conditions

The differential flow pattern maps show the limit of the well-posedness of the equation system, the neutral stability curves at the initial conditions, and the regions where the stratified and non-stratified flow can occur. The neutral stability curves can coincide with the VKH criteria for horizontal and slightly inclined pipes (see Section 2.3.2).

Downward-inclined pipes have a stabilizing effect on fluid flow. According to Issa and Kempf (2003), this is why downward inclined pipes are usually placed before upward inclined pipes. The unstable region is located between the IKH and VKH limits. It represents the zone where it is most probable that stratified wavy flow occurs and, in some circumstances, intermittent flow. This criterion must be validated through the stability analysis of the semi-discretized equations (see Section 3.3) and transient simulations.

Fig 23 validates a differential flow pattern map of horizontal pipes with the map obtained in Sanderse, Smith and Hendrix (2017). The system can be well-posed and unstable at lower superficial velocities at the initial conditions. The governing equations (4.1) to (4.4) do not consider the second term of the hydrostatic pressure term of Sanderse, Smith and Hendrix (2017) since it is third order.

3.4.2 Discrete and hybrid flow pattern maps

As the first approach, we simulate air-water flow ($\rho_l = 1000$ kg/m^3, $\mu_l = 1.8e-5$ Pa s, $\mu_g = 8.9e-4$ Pa s) in a horizontal pipe with $D = 0.078$ m, $L = 1$ m, and $n = 40$ elements. Wave growth simulations and the construction of fully discretized flow pattern maps (see Figs. 24 and 25) are performed simultaneously to track the stability of the equations within the entire domain. A characteristics analysis is performed parallel to the numerical model to ensure that the computations made with this numerical model correspond to physical phenomena.

The Discrete Flow Pattern Maps are constructed like differential flow pattern maps in Section 3.4, using a sequence of superficial liquid and gas velocities, solving the discrete equations with a small perturbation as the initial condition, and determining the growth rate ω_N. The stability boundary is given by $\text{Im}(\omega_N) = 0$. Additionally, when amplification factors $0 \leq G(z) \leq 1$ are found, the system is unstable; alternatively, the system is stable when amplification factors $G(z) > 1$ are found. The computations are stopped when $0 \leq G(z) \leq 1$.

The amplification factors of the fully discrete equations are computed for the time step $\Delta t = 1/40\ s$ as the first approach, as suggested in (Sanderse; Smith; Hendrix, 2017). Also, the CFL number is $C_{\text{CFL}} = 1$, and then it is adjusted following the procedure of (Sanderse; Smith; Hendrix, 2017). The well-posedness of the fully discrete equations is evaluated every

time step, so simulations starting above the limit of ill-posedness are directly considered ill-posed.

Hybrid flow pattern maps in Figs. 23 to 25 depict a combination of neutral stability and limit of well-posedness curves belonging to differential, discrete, and experimental flow pattern maps for a large sequence of initial conditions and local inclinations (see Figs. 24 and 25). A well-posedness analysis was performed at each time step, Since the Two-fluid Model is ill-posed for high slip velocities (i.e., where slug flow takes place). The stability analysis determines the feasibility of simulating wave growth with higher-order finite-element methods.

Sanderse, Smith and Hendrix (2017) stated that any simulation starting above the ill-posedness boundary would be marked as ill-posed because our ill-posedness indicator is based on evaluating the eigenvalues of the differential equations. However, simulations that start in the unstable well-posed regime may grow into the ill-posed regime due to nonlinear effects. The regions and the curves illustrated in Fig. 25 agree with differential and experimental flow pattern maps. For a well-posed unstable initial condition, the system has a maximum numerical growth $G_{\text{max}} = 1.00212604$ and $\omega_{\text{max}} = 0.386$ the first $10s$ of simulation.

The hybrid flow pattern maps at the initial conditions, shown in Figs. 24 and 25, present good agreement with the literature. However, the discrepancies at high flow velocities may have been triggered due to several reasons. One of these reasons is the lack of accurate closure models in terms of the primitive variables of the equation system. The Two-fluid Model equation system in this thesis uses phenomenological correlations to describe friction, which can lead to divergences at high flow rates.

Figure 23 – Differential flow pattern maps validated with the maps in Table 4.

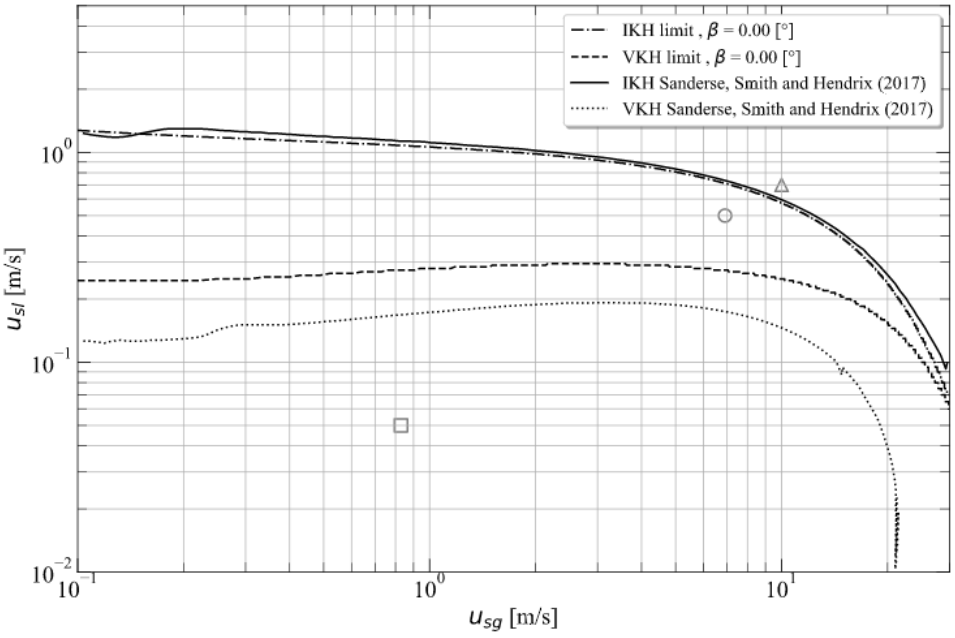

Note: 1 m horizontal pipe ($\beta = 0\ deg$) with $D = 0.078\ m$.

Figure 24 – Hybrid flow pattern maps for horizontal pipes ($\beta = 0\ deg$) with $D = 0.078\ m$

(a) Discrete flow pattern maps in horizontal pipes $(\beta = 0)$.

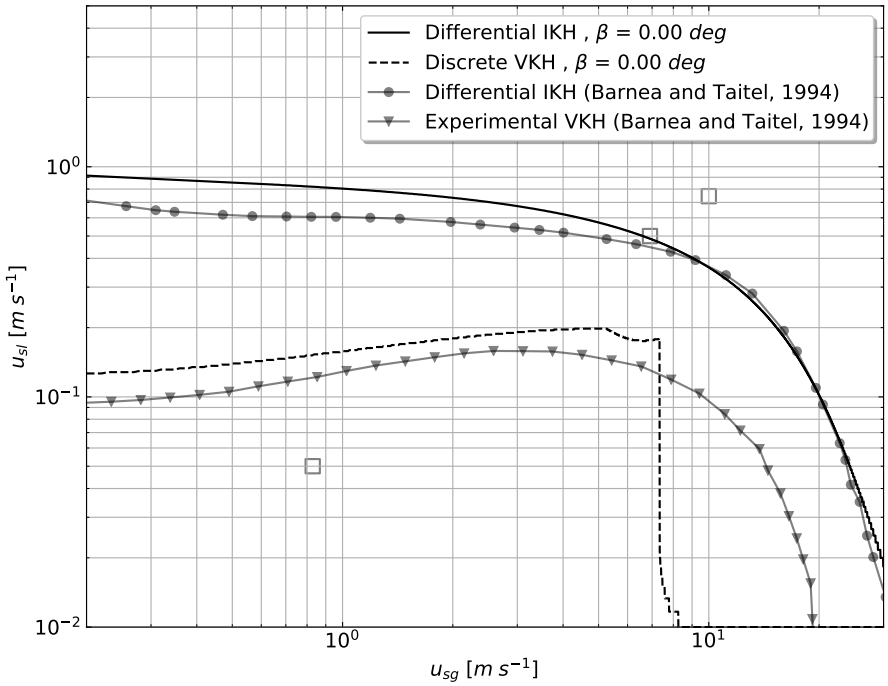

(b) Discrete flow pattern maps in upward inclinedpipes ($\beta = 0.25\ deg$).

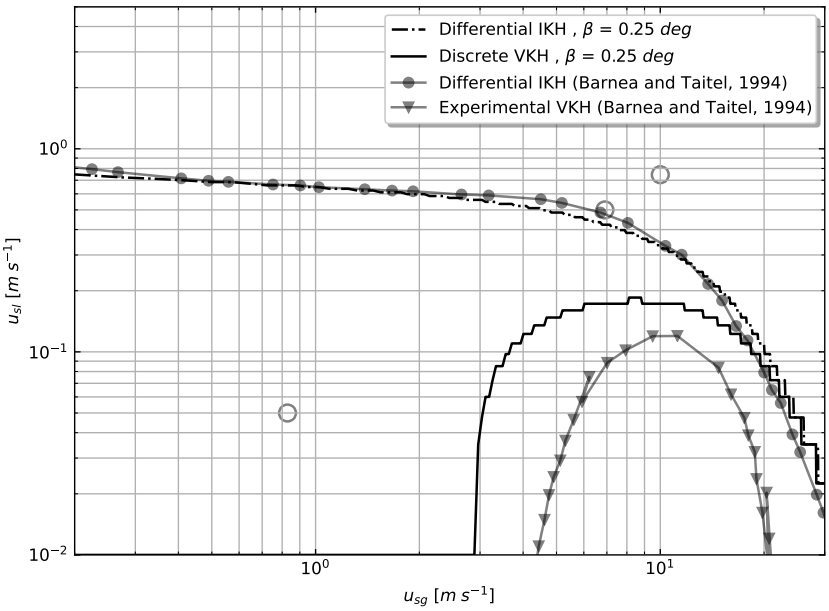

Note: Taylor-Hood $\mathcal{P}_2$ finite elements for the convective and source terms and the BDF2 scheme for time integration. Validated with the maps of Barnea and Taitel (1994)

The main advantage of constructing hybrid flow pattern maps is that the theoretical and factual stability regions and potential transitions can be tracked at each time step, revealing several issues related to the numerical model, including morphology changes in the maps and displacements of the limits. These alterations during transient simulations may suggest, among other reasons, the limitations of certain closure relations, numerical discretization schemes, geometrical discontinuities, or even regularization mechanisms. As shown in Figs. 23 to 25, discrepancies between theoretical and numerical curves can be tracked in time in order to understand their causes and analyze the divergences that can appear during long simulation times. The results of this thesis depict an adoption of the methodology for constructing Discrete Flow Pattern Maps for horizontal pipes and Finite-volume methods, detailed in (Sanderse; Smith; Hendrix, 2017), for an open-source Taylor-Hood finite-element model with the possibility of conducting studies on more complex geometries and discretization schemes.

Figure 25 – Hybrid flow pattern maps for pipes with $D = 0.078\ m$

(a) Downward inclinedpipes ($\beta = -5\ deg$).

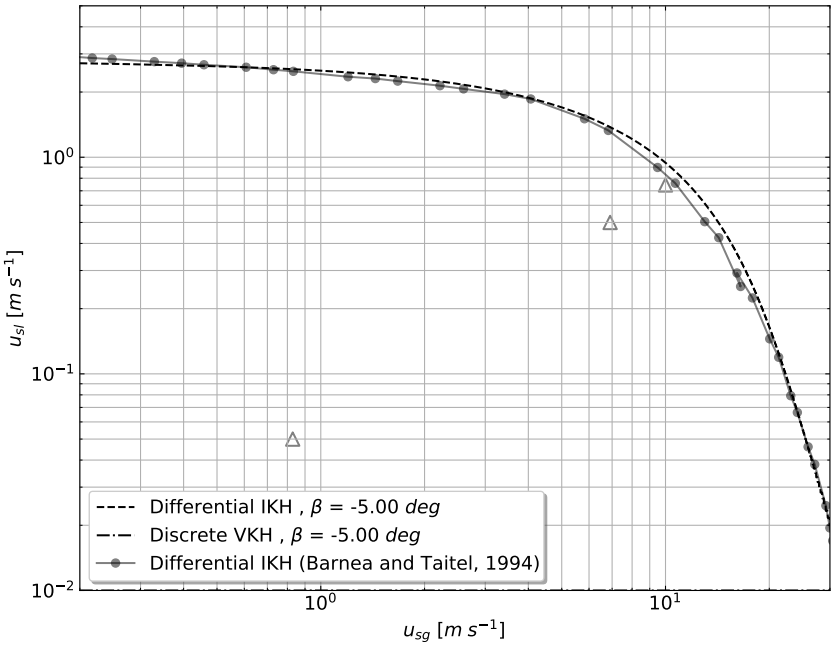

Note: Taylor-Hood $\mathcal{P}_2$ finite elements for the convective and source terms and the BDF2 scheme for time integration. Validated with the maps of Barnea and Taitel (1994).

4 CONCLUSIONS AND FUTURE WORK

This chapter presents the conclusions and the next steps, conforming with the objective, hypothesis, and methods described in Chapter 1.

4.1 Conclusions

This thesis presents an analysis of the capability of a novel finite-element formulation, combined with linear stability analysis, for predicting wave growth with the Two-fluid Model. The numerical formulation predicts well-posedness and wave growth that may lead to flow pattern transition for a range of superficial velocities, pipe diameters, and pipe inclinations. Although the previous works investigating wave growth in stratified smooth flows and their consequent onset of flow pattern transitions have proposed diverse numerical formulations and regularization mechanisms, the solution to the one-dimensional Two-fluid Model still represents an open question.

The Two-fluid Model is conditionally well-posed; therefore, predicting well-posedness during flow simulations is fundamental during wave growth, flow pattern transitions, and the onset of slugging. The differential flow pattern maps based on Kelvin-Helmholtz instabilities show the stability and well-posedness regime regions, predicting potential flow pattern transitions.

The stiffness analysis demonstrated that several factors (e.g., mesh size, local pipe inclination, order of basis functions, and average phase velocities) could affect the eigenvalue distribution of semi-discrete equations, presenting unstable modes that may lead to wave growth. Eigenspectra shows that convective waves are not attenuated by numerical diffusion present in the numerical schemes. Also, the eigenvalues associated with acoustic waves do not affect wave growth for smooth initial conditions.

Although continuous Galerkin elements for the spatial discretization predict wave growth under well-posed unstable initial conditions, Taylor-Hood elements preserve the inf-sup stability condition and provide the possibility of using higher-order basis functions. Also, Taylor-Hood elements maintain the eigenstructure and stability regions predicted through Fourier analysis of the differential equations. Furthermore, Mini-enriched stabilized elements reproduce wave growth but are limited to lower-order basis functions.

The fully discrete flow pattern maps track the actual stability properties of the numerical formulation within the entire domain during the first time steps of transient simulations, not only in horizontal pipes as in previous studies but in slightly inclined pipes. The numerical formulation presents the capability for adding diverse closure relations (i.e., regularization terms for high flow rates, a local variation of inclination angle along the pipeline) into the variational form, being advantageous over the finite volume method, as in some of the previous studies.

In slightly inclined pipes and stratified smooth flow as the initial condition, continuous finite-element schemes render expected wave growth rates in agreement with the literature. However, special attention must be put when simulating wave growth when discontinuities appear during single to two-phase flow transitions and in complex configurations composed of irregular geometries.

For further investigations, the numerical Model can perform linear stability analysis for distinct equation systems as inputs. This enables linear stability studies of regularized equation systems by adding physical and numerical terms from the literature. Also, the Model allows the incorporation of other finite element spaces available in the open-source computing FEniCS Project platform, enabling the study of stiffness of different discretization techniques for initial conditions related to higher gas and liquid superficial velocities.

4.2 Future work

Future work concerns a further analysis of numerical methods, regularization techniques, transition prediction, verification, and numerical model validation for solving the Two-fluid Model proposed in this thesis. The Model proposed uses the Slug Capturing approach as a reference. Therefore, the next steps consist of simulating factual flow-pattern transitions considering the effects of nonlinear instabilities.

Regarding numerical modeling, the literature shows recent works on Discontinuous Galerkin methods for solving convection-dominated problems with discontinuities. For instance, The transport level-set problem can be solved with Discontinuous Galerkin methods, and the transport equations can be discretized with Taylor-Hood elements, as inspired by the technique of Bezchlebová, Dolejš\'\i and Feistauer (2016). Besides, space-time adaptive techniques may be an option for further studies during factual transitions.

For high gas-liquid relative velocities, the equations become ill-posed. Thus, it is essential to study physical and numerical regularization mechanisms. The addition of level-set equations for the interface can be investigated to obtain larger unstable, well-posedness regions in the fully discrete flow pattern maps presented in this work. Furthermore, to avoid *ad hoc* analyses for the addition of numerical viscosity as regularization, we can investigate other numerical regularization techniques that may extend the well-posedness regions and, in consequence, improve the capability of simulating wave growth under higher flow rates.

Studies on the dispersive effect of the two-fluid model equations using Taylor-Hood elements for the spatial derivatives can be complementary. For example, the excessive growth rate of disturbances can be attenuated at a cut-off criterion: the minimum size of the elements (Montini, 2010).

This thesis presents solutions under the ill-posedness limits and before flow pattern transitions. In the future, we can consider transition criteria to deal with the gas discontinuities in the pipelines during the one-phase to two-phase switch in stratified to intermittent flow

transitions. In terms of wave growth and transition simulations, the influence of acoustic waves on stability and wave growth might be investigated since, in this study, we only associate the effect of convective waves on wave growth.

How the Model is constructed enables adding tests for field conditions and verification with equation systems with properties similar to the Two-fluid Model equations. Also, the Model can include demos related to pipe inclinations found in receiving facilities for further studies.

BIBLIOGRAPHY

Agrawal, S. S.; Gregory, G. A.; Govier, G. W. An analysis of horizontal stratified two phase flow in pipes. *The Canadian Journal of Chemical Engineering*, Wiley Online Library, v. 51, n. 3, p. 280–286, 1973.

Alnæs, M. S. et al. The FEniCS Project Version 1.5. *Archive of Numerical Software*, v. 3, n. 100, 2015.

Alnæs, M. S. et al. Unified form language: A domain-specific language for weak formulations of partial differential equations. *ACM Transactions on Mathematical Software (TOMS)*, ACM, v. 40, n. 2, p. 9, 2014.

Anderson, D. A.; Tannehill, J. C.; Pletcher, R. H. *Computational fluid mechanics and heat transfer*. : Taylor & Francis, 1997.

Ansari, M. R. Dynamical behavior of slug initiation generated by short waves in two-phase air-water stratified flow. *ASME HEAT TRANSFER DIV PUBL HTD*, v. 361, p. 289–296, 1998.

Ansari, M. R.; Daramizadeh, A. Slug type hydrodynamic instability analysis using a five equations hyperbolic two-pressure, two-fluid model. *Ocean Engineering*, Elsevier, v. 52, p. 1–12, 2012.

Ansari, M. R.; Shokri, V. Numerical modeling of slug flow initiation in horizontal channels using a two-fluid model. *International Journal of Heat and Fluid Flow*, Elsevier Inc., v. 32, n. 1, p. 145–155, 2011.

Arnold, D. N.; Franco, B.; Fortin, M. A stable finite element for the Stokes equations. *Calcolo*, Springer, v. 21, n. 4, p. 337–344, 1984.

Balay, S. et al. PETSc users manual. Argonne National Laboratory, 2019.

Balay, S. et al. Efficient management of parallelism in object-oriented numerical software libraries. In: *Modern software tools for scientific computing*. : Springer, 1997. p. 163–202.

Barclay, G. J.; Griffiths, D. F.; Higham, D. J. Theta method dynamics. *LMS Journal of Computation and Mathematics*, Cambridge University Press, v. 3, p. 27–43, 2000.

Barnea, D.; Shoham, O.; Taitel, Y. Flow pattern transition for downward inclined two phase flow; horizontal to vertical. *Chemical Engineering Science*, Elsevier, v. 37, n. 5, p. 735–740, 1982.

Barnea, D. et al. Gas-liquid flow in inclined tubes: flow pattern transitions for upward flow. *Chemical Engineering Science*, Pergamon, v. 40, n. 1, p. 131–136, 1985.

Barnea, D.; Taitel, Y. Interfacial and structural stability of separated flow. *International Journal of Multiphase Flow*, v. 20, n. SUPPL. 1, p. 387–414, 1994.

Bendiksen, K. et al. Dynamic simulation of multiphase transportation systems. In: *Multiphase Technology and Consequences for Field Development Forum, Stavanger, Norway*. 1987.

Bendiksen, K.; Espedal, M. Onset of slugging in horizontal gas-liquid pipe flow. *International journal of multiphase flow*, Elsevier, v. 18, n. 2, p. 237–247, 1992. ISSN 03019322.

Bendlksen, K. H. et al. The dynamic two-fluid model OLGA: Theory and application. *SPE production engineering*, Society of Petroleum Engineers, v. 6, n. 02, p. 171–180, 1991. ISSN 08859221.

Bertodano, M. L. D. et al. *Two-fluid model stability, simulation and chaos*. : Springer, 2017. 1–358 p.

Bertodano, M. Lopez-de; Fullmer, W.; Vaidheeswaran, A. One-dimensional two-equation two-fluid model stability. *Multiphase Science and Technology*, Begel House Inc., v. 25, n. 2-4, 2013.

Bezchlebová, E.; Dolejš\'\i, V.; Feistauer, M. Discontinuous Galerkin method for the solution of a transport level-set problem. *Computers & Mathematics with Applications*, Elsevier, v. 72, n. 3, p. 455–480, 2016.

Bezchlebová, E. et al. Numerical simulation of two-phase flow of immiscible fluids by the finite element, discontinuous Galerkin and level-set methods. *Advances in Computational Mathematics*, Springer, v. 45, n. 4, p. 1993–2018, 2019.

Biberg, D. An explicit approximation for the wetted angle in two-phase stratified pipe flow. *Canadian Journal of Chemical Engineering*, Wiley Online Library, v. 77, n. 6, p. 1221–1224, 1999.

Black, P. S. et al. Studying transient multi-phase flow using the pipeline analysis code (PLAC). 1990.

Boffi, D. Three-dimensional finite element methods for the Stokes problem. *SIAM Journal on Numerical Analysis*, SIAM, v. 34, n. 2, p. 664–670, 1997.

Bonizzi, M. *Transient one-dimensional modelling of multiphase slug flows*. 1–310 p. Tese (Doutorado) — Department of Mechanical Engineering, Imperial College London, 2003. Available on: https://core.ac.uk/download/pdf/1589263.pdf.

Bonzanini, A.; Picchi, D.; Poesio, P. Simplified 1d incompressible two-fluid model with artificial diffusion for slug flow capturing in horizontal and nearly horizontal pipes. *Energies*, Multidisciplinary Digital Publishing Institute, v. 10, n. 9, p. 1372, 2017.

Courant, R.; Friedrichs, K.; Lewy, H. Über die partiellen Differenzengleichungen der mathematischen Physik. *Mathematische annalen*, Springer, v. 100, n. 1, p. 32–74, 1928.

Courant, R.; Friedrichs, K.; Lewy, H. On the partial difference equations of mathematical physics. *IBM Journal of Research and Development*, IBM, v. 11, n. 2, p. 215–234, 2010.

Davis, T. A. Algorithm 832: UMFPACK V4. 3—an unsymmetric-pattern multifrontal method. *ACM Transactions on Mathematical Software (TOMS)*, ACM New York, NY, USA, v. 30, n. 2, p. 196–199, 2004.

Dinh, T. N.; Nourgaliev, R. R.; Theofanous, T. G. Understanding the ill-posed two-fluid model. In: *Proceedings of the 10th international topical meeting on nuclear reactor thermal-hydraulics (NURETH'03)*. 2003. p. 1–37.

Dodd, R. K. et al. *Solitons and nonlinear wave equations*. 1982. 630 p. Available on: https://www.osti.gov/biblio/6349564.

Drew, D. A. Mathematical modeling of two-phase flow. *Annual review of fluid mechanics*, Annual Reviews 4139 El Camino Way, PO Box 10139, Palo Alto, CA 94303-0139, USA, v. 15, n. 1, p. 261–291, 1983.

Drew, D. A.; Passman, S. L. Theory of multicomponent fluids. 1999. *Applied Mathematical Sciences*, 1998.

Duff, I. S.; Scott, J. A. A parallel direct solver for large sparse highly unsymmetric linear systems. *ACM Transactions on Mathematical Software (TOMS)*, ACM New York, NY, USA, v. 30, n. 2, p. 95–117, 2004.

Evje, S.; Flåtten, T. Hybrid flux-splitting schemes for a common two-fluid model. *Journal of Computational Physics*, Elsevier, v. 192, n. 1, p. 175–210, 2003.

Ferrari, M.; Bonzanini, A.; Poesio, P. A 5-equation, transient, hyperbolic, 1-dimensional model for slug capturing in pipes. *International Journal for Numerical Methods in Fluids*, Wiley Online Library, v. 85, n. 6, p. 327–362, 2017.

Fick, A. Uber diffusion. *Annalen der Physik*, n. 170, p. 59–86, 1855.

Fletcher, C. A. J. *Computational techniques for fluid dynamics 2: Specific techniques for different flow categories*. : Springer Science & Business Media, 2012.

Fullmer, W. D. *Dynamic simulation of wavy-stratified two-phase flow with the one-dimensional two-fluid model*. Tese (Doutorado) — Purdue University, 2014.

Fullmer, W. D. et al. Analysis of stability, verification and chaos with the Kreiss–Yström equations. *Applied Mathematics and Computation*, Elsevier, v. 248, p. 28–46, 2014.

Fullmer, W. D. et al. Linear and nonlinear analysis of the Kelvin-Helmholtz instability with the 1D two-fluid model. In: *Proc. 7th International Conference on Multiphase Flow*. 2010.

Hadamard, J. Sur les problemes aux derivees partielles et leur signification physique Bull Univ Princeton 13: 49–52. *Find this article online*, 1902.

Han, P.; Guo, L. Numerical simulation of terrain-induced severe slugging coupled by hydrodynamic slugs in a pipeline–riser system. *International Journal of Heat and Fluid Flow*, Elsevier, v. 56, p. 355–366, 2015.

Hand, N. P. *Gas liquid co-current flow in a horizontal pipe.* Tese (Doutorado) — Queen's University of Belfast, 1991.

Hendrix, M. H. W. et al. Comparison of numerical methods for slug capturing with the two-fluid model. In: *ICMF-2016 - 9th International Conference on Multiphase Flow May 22nd - 27th 2016, Firenze, Italy*. 2016.

Hirsch, C. *Numerical computation of internal and external flows: Computational methods for inviscid and viscous flows*. : John Wiley & Sons, 1988. v. 2.

Hirsch, C. *Numerical computation of internal and external flows: The fundamentals of computational fluid dynamics, vol 1*. : Elsevier, 1988.

Holmås, H. et al. Analysis of a 1D incompressible two-fluid model including artificial diffusion. *IMA journal of applied mathematics*, Oxford University Press, v. 73, n. 4, p. 651–667, 2008. ISSN 02724960.

Husain, A.; WG, C. Applicability of the homogeneous flow model to two-phase pressure drop in straight pipe and across area changes. 1978.

Ishii, M. *Thermo-fluid dynamic theory of two-phase flow*. : Paris: Eyrolles, 1975. (Collection de la Direction des études et recherches d'Electricité de France, 22.).

Issa, R. I.; Kempf, M. H. W. Simulation of slug flow in horizontal and nearly horizontal pipes with the two-fluid model. *International Journal of Multiphase Flow*, Elsevier, v. 29, n. 1, p. 69–95, 2003.

Katz, R. F. et al. Numerical simulation of geodynamic processes with the Portable Extensible Toolkit for Scientific Computation. *Physics of the Earth and Planetary Interiors*, Elsevier, v. 163, n. 1-4, p. 52–68, 2007.

Kim, J.; Kang, K.; Lowengrub, J. Conservative multigrid methods for cahn-hilliard fluids. *Journal of Computational Physics*, Elsevier, v. 193, n. 2, p. 511–543, 2004.

Kjeldby, T.; Nydal, O. A lagrangian three-phase slug tracking framework. *International journal of multiphase flow*, Elsevier, v. 56, p. 184–194, 2013.

Lazo-Vásquez, D.; Baliño, J. L. On the use of continuous finite-elements for two-phase flow simulations in horizontal and nearly horizontal pipes. In: *ANAIS DO III CONGRESSO BRASILEIRO DE FLUIDODINÂMICA COMPUTACIONAL, 2022*. 2022. ISSN 2525-4472. Available on: https://proceedings.science/cbcfd-2022/trabalhos/on-the-use-of-continuous-finite-elements-for-two-phase-flow-simulations-in-horiz?lang=pt-br.

Lazo-Vásquez, D.; Baliño, J. L. Prediction of flow pattern transition in pipelines using Taylor-Hood finite elements. In: *ICMF-2023 - 11th International Conference on Multiphase Flow April 2nd - 7th 2023, Kobe, Japan*. 2023.

Lazo-Vásquez, D.; Baliño, J. L. Two-fluid model simulations sample code. GitHub repository - Zenodo, 2023. Available on: https://zenodo.org/record/8025614.

Lehoucq, R. B.; Sorensen, D. C.; Yang, C. *ARPACK users' guide: solution of large-scale eigenvalue problems with implicitly restarted Arnoldi methods*. : SIAM, 1998. 1-7 p.

LeVeque, R. J. *Finite volume methods for hyperbolic problems*. : Cambridge university press, 2002. v. 31.

Liao, J.; Mei, R.; Klausner, J. F. A study on the numerical stability of the two-fluid model near ill-posedness. *International Journal of Multiphase Flow*, v. 34, n. 11, p. 1067–1087, 2008.

Lin, P. Y.; Hanratty, T. J. Prediction of the initiation of slugs with linear stability theory. *International Journal of Multiphase Flow*, v. 12, n. 1, p. 79–98, 1986.

Logg, A.; Mardal, K. A.; Wells, G. *Automated Solution of Differential Equations by the Finite Element Method: The FEniCS Book*. : Springer Science and Business Media, 2012. 718 p.

Masella, J. M. et al. Transient simulation of two-phase flows in pipes. *International Journal of Multiphase Flow*, Elsevier, v. 24, n. 5, p. 739–755, 1998.

McQuillan, K. W.; Whalley, P. B. Flow patterns in vertical two-phase flow. *International Journal of Multiphase Flow*, Elsevier, v. 11, n. 2, p. 161–175, 1985.

Mercier, B. *Topics in Finite Element Solution of Elliptic Problems*. : Springer, 1979. 92–144 p.

Montini, M. *Closure relations of the one-dimensional two-fluid model for the simulation of slug flows*. 241 p. Tese (Doutorado) — Imperial College London, 2010. Available on: https://core.ac.uk/download/pdf/1589263.pdf.

Morais, J. M. d. Petróleo em águas profundas: uma história tecnológica da Petrobras na exploração e produção offshore. Instituto de Pesquisa Econômica Aplicada (IPEA), 2013.

Munkejord, S. T.; Gran, I. R. *Modelling and Numerical Methods for Two-Phase Flow, vol*. Tese (Doutorado) — Phd Thesis 2005, NTNU, Trondheim, Norway. VDM Verlag Dr. Müller Aktiengesell˜. . . , 2009.

Ortega, A. J.; Nieckele, A. O. Simulation of horizontal two-phase slug flows using the two-fluid model with a conservative and non-conservative formulation. In: *Proceedings of COBEM*. 2005.

Pellegrini, S. et al. Sample-based prior using a phenomenological model for slug flow. In: *ICMF-2019 - 10th International Conference on Multiphase Flow April 19th - 24th 2019, Rio de Janeiro, Brazil*. 2019.

Pokharna, H.; Mori, M.; Ransom, V. H. Regularization of two-phase flow models: A comparison of numerical and differential approaches. *Journal of Computational Physics*, Elsevier, v. 134, n. 2, p. 282–295, 1997.

Ramshaw, J. D.; Trapp, J. A. Characteristics, stability, and short-wavelength phenomena in two-phase flow equation systems. *Nuclear Science and Engineering*, Taylor & Francis, v. 66, n. 1, p. 93–102, 1978.

Rossum, G. V.; Drake, F. L. *Python 3 Reference Manual*. Scotts Valley, CA: CreateSpace, 2009. ISBN 1441412697.

Sanderse, B.; Smith, I. E.; Hendrix, M. H. Analysis of time integration methods for the compressible two-fluid model for pipe flow simulations. *International Journal of Multiphase Flow*, v. 95, p. 155–174, 2017.

Schlumberger. *Olifield Glossary*. 2020. Available on: https://www.glossary.oilfield.slb.com/en.

Shoham, O. *Flow Pattern Transition and Characterization in Gas-Liquid Two-Phase Flow in Inclined Pipes*. Tese (Doutorado) — Tel Aviv University, 1982. Available on: https://www.worldcat.org/title/flow-pattern-transition-and-characterization-in-gas-liquid-two-phase-flow-in-inclined-pipes/oclc/731727076.

Smith, I. E. *A 7-field Lagrangian slug capturing and slug tracking model with higher order methods*. Tese (Doutorado) — NTNU, 2017. Available on: https://ntnuopen.ntnu.no/ntnu-xmlui/handle/11250/2455762.

Taitel, Y.; Barnea, D. A consistent approach for calculating pressure drop in inclined slug flow. *Chemical Engineering Science*, v. 45, n. 5, p. 1199–1206, 1990. ISSN 00092509.

Taitel, Y.; Barnea, D. Effect of gas compressibility on a slug tracking model. *Chemical Engineering Science*, Elsevier, v. 53, n. 11, p. 2089–2097, 1998. ISSN 00092509.

Taitel, Y. et al. Modelling flow pattern transitions for steady upward gas-liquid flow in vertical tubes. *AIChE Journal*, Wiley Online Library, v. 26, n. 3, p. 345–354, 1980. ISSN 15475905.

Taitel, Y.; Dukler, A. E. A model for predicting flow regime transitions in horizontal and near horizontal gas-liquid flow. *AIChE Journal*, Wiley Online Library, v. 22, n. 1, p. 47–55, 1976.

Taylor, C.; Hood, P. A numerical solution of the navier-stokes equations using the finite element technique. *Computers and Fluids*, Elsevier, v. 1, n. 1, p. 73–100, 1973.

Taylor, R. L.; Zienkiewicz, O. C. *The finite element method*. : Butterworth-Heinemann, 2013.

Versteeg, H. K.; Malalasekera, W. *An introduction to computational fluid dynamics: the finite volume method*. : Pearson education, 2007.

VonNeumann, J.; Richtmyer, R. D. A method for the numerical calculation of hydrodynamic shocks. *Journal of applied physics*, American Institute of Physics, v. 21, n. 3, p. 232–237, 1950.

Wallis, G. B.; Wallis. One-dimensional two-phase flow. McGraw-Hill, 1969.

Wolfram Research, Inc. *Mathematica, Version 12.0*. 2020.

Z.Fan, Z.; Ruder; Hanratty, T. J. Pressure profiles for slugs in horizontal pipelines. *International Journal of Multiphase Flow*, Elsevier, v. 19, n. 3, p. 421–437, 1993.

Zheng, G.; Brill, J. P.; Taitel, Y. Slug flow behavior in a hilly terrain pipeline. *International journal of multiphase flow*, Elsevier, v. 20, n. 1, p. 63–79, 1994. ISSN 03019322.

Zwieten, J. van et al. Efficient simulation of one-dimensional two-phase flow with a high-order h-adaptive space-time discontinuous galerkin method. *Computers & Fluids*, Elsevier, v. 156, p. 34–47, 2017.

APPENDIX 1 - DERIVATION OF THE TWO-FLUID MODEL IN MATRIX FORM

The complete Two-fluid Model (Bonizzi, 2003; Sanderse; Smith; Hendrix, 2017; Smith, 2017; Zwieten et al., 2017) (i.e., Eqs. (2.1)-(2.4)) reads:

Continuity

$$\partial_t \left(\alpha_l \rho_l\right) + \partial_{\mathbf{s}} \left(\alpha_l \rho_l u_l\right) = 0 \tag{4.1}$$

$$\partial_t \left(\alpha_g \rho_g\right) + \partial_{\mathbf{s}} \left(\alpha_g \rho_g u_g\right) = 0 \tag{4.2}$$

Momentum

$$\begin{aligned} \partial_t \left(\alpha_l \rho_l u_l\right) + \partial_{\mathbf{s}} \left(\alpha_l \rho_l u_l^2\right) + \alpha_l \partial_{\mathbf{s}} p_{il} + \alpha_l \rho_l g \partial_{\mathbf{s}} h_l \cos\beta \\ = -\alpha_l \rho_l g \sin\beta - F_{lw} + F_{gl} \end{aligned} \tag{4.3}$$

$$\begin{aligned} \partial_t \left(\alpha_g \rho_g u_g\right) + \partial_{\mathbf{s}} \left(\alpha_g \rho_g u_g^2\right) + \alpha_g \partial_{\mathbf{s}} p_{ig} + \alpha_g \rho_g g \partial_{\mathbf{s}} h_l \cos\beta \\ = -\alpha_g \rho_g g \sin\beta - F_{gw} - F_{gl} \end{aligned} \tag{4.4}$$

If the compressibility of the gas phase is taken into account, the matrices $\mathbf{A}(\mathbf{W})$, $\mathbf{B}(\mathbf{W})$ and $\mathbf{C}(\mathbf{W})$ are:

$$\mathbf{A}(\mathbf{W}) = \begin{pmatrix} \rho_l & 0 & 0 & 0 \\ -\left(\frac{p_i - p_{i,0}}{c_g^2} + \rho_{g,0}\right) & 0 & 0 & \frac{1}{c_g^2}\left(1-\alpha_l\right) \\ \rho_l u_l & \rho_l \alpha_l & 0 & 0 \\ -\left(\frac{p_i - p_{i,0}}{c_g^2} + \rho_{g,0}\right) u_g & 0 & \left(\frac{p_i - p_{i,0}}{c_g^2} + \rho_{g,0}\right)\left(1-\alpha_l\right) & \frac{1}{c_g^2}\left(1-\alpha_l\right) u_g \end{pmatrix} \tag{4.5}$$

$$\mathbf{B}(\mathbf{W}) = \begin{pmatrix} \rho_l u_l & \rho_l \alpha_l & 0 & 0 \\ -\left(\frac{p_i - p_{i,0}}{c_g^2} + \rho_{g,0}\right) u_g & 0 & \left(\frac{p_i - p_{i,0}}{c_g^2} + \rho_{g,0}\right)\left(1-\alpha_l\right) & \frac{1}{c_g^2}\left(1-\alpha_l\right) u_g \\ \rho_l u_l^2 - \alpha_l \rho_l d_c g & 2\rho_l \alpha_l u_l & 0 & \alpha_l \\ \left(\frac{p_i - p_{i,0}}{c_g^2} + \rho_{g,0}\right)\left(-u_g^2 - d_c\left(1-\alpha_l\right) g\right) & 0 & \left(\frac{p_i - p_{i,0}}{c_g^2} + \rho_{g,0}\right) 2\left(1-\alpha_l\right) u_g & \frac{1}{c_g^2}\left(1-\alpha_l\right) u_g^2 + \left(1-\alpha_l\right) \end{pmatrix} \tag{4.6}$$

$$\mathbf{C}(\mathbf{W}) = \begin{pmatrix} 0 \\ 0 \\ -\rho_l g \alpha_l \sin\beta - F_{lw} + F_{gl} \\ -\left(\frac{p_i - p_{i,0}}{c_g^2} + \rho_{g,0}\right) g\left(1-\alpha_1\right) \sin\beta - F_{gw} - F_{gl} \end{pmatrix} \tag{4.7}$$

APPENDIX 2 - LINEARIZATION OF THE TWO-FLUID MODEL

The conservative form of the Two-fluid Model (i.e., Eqs. (2.1)-(2.4)) is derived as follows:

$$\frac{\partial \mathbf{U}}{\partial t} + \mathbf{B}(\mathbf{W})\frac{\partial \mathbf{W}}{\partial \mathbf{U}}\frac{\partial \mathbf{U}}{\partial \mathbf{s}} = \mathbf{C}(\mathbf{W}). \tag{4.8}$$

where $\mathbf{U}$ is the vector of the conserved variables and $\mathbf{W}$ is the vector of the primitive variables. Equation 4.8 can be written as:

$$\frac{\partial \mathbf{U}}{\partial t} + \mathbf{B}(\mathbf{W})\left[\frac{\partial \mathbf{U}}{\partial \mathbf{W}}\right]^{-1}\frac{\partial \mathbf{U}}{\partial \mathbf{s}} = \mathbf{C}(\mathbf{W}), \tag{4.9}$$

where

$$\mathbf{E}(\mathbf{W}) = \mathbf{B}(\mathbf{W})\left[\frac{\partial \mathbf{U}}{\partial \mathbf{W}}\right]^{-1} = \begin{pmatrix} u_l & 0 & 0 & 0 \\ \frac{\rho_g u_g u_l}{\alpha_l \rho_l} & 0 & \frac{\alpha_g \rho_g}{\alpha_l \rho_l} & 0 \\ 0 & -\frac{2\alpha_l \rho_l u_g u_l}{\alpha_g \rho_g} & 0 & \frac{\alpha_l}{\alpha_g \rho_g} \\ -\frac{\rho_g^2\left(u_g^2 + \alpha_g g d_c\right)}{\alpha_g \rho_l} & 0 & 0 & 0 \end{pmatrix} \tag{4.10}$$

By defining $\mathbf{W}$ in terms of $\mathbf{U}$:

$$\begin{aligned} \alpha_l &= \frac{1}{\rho_l}\mathbf{W}_1, \\ u_l &= \frac{\mathbf{W}_3}{\mathbf{W}_1}, \\ u_g &= \frac{\mathbf{W}_4}{\mathbf{W}_2}, \\ p_i &= p_{i,0} + c_g^2\left(-\rho_{g,0} + \rho_l\frac{\mathbf{W}_2}{\mathbf{W}_1}\right), \end{aligned} \tag{4.11}$$

The elements of the matrix $\mathbf{B}(\mathbf{U})$ of the conservative form of the Two-fluid Model become:

$$\begin{aligned} \mathbf{B_{11}}(\mathbf{U}) &= \frac{\mathbf{W}_3}{\mathbf{W}_1} \\ \mathbf{B_{21}}(\mathbf{U}) &= \frac{\rho_l \mathbf{W}_3 \mathbf{W}_4}{\mathbf{W}_1^3} \\ \mathbf{B_{23}}(\mathbf{U}) &= \frac{\left(\rho_l - \mathbf{W}_1\right)\mathbf{W}_2}{\mathbf{W}_1^2} \\ \mathbf{B_{32}}(\mathbf{U}) &= \frac{2\mathbf{W}_1 \mathbf{W}_3 \mathbf{W}_4}{\left(-\rho_l + \mathbf{W}_1\right)\mathbf{W}_2^2} \\ \mathbf{B_{34}}(\mathbf{U}) &= \frac{\mathbf{W}_1^2}{\rho_l^2 \mathbf{W}_2 - \rho_l \mathbf{W}_1 \mathbf{W}_2} \\ \mathbf{B_{41}}(\mathbf{U}) &= \frac{\rho_l\left(-\rho_l \mathbf{W}_4^2 + g\left(-\rho_l + \mathbf{W}_1\right)\mathbf{W}_2^2 d_c\right)}{\left(\rho_l - \mathbf{W}_1\right)\mathbf{W}_1^2} \end{aligned} \tag{4.12}$$

APPENDIX 3 - DERIVATION OF THE QUASILINEAR FORM OF THE TWO-FLUID MODEL

The Two-fluid Model (i.e., Eqs. (2.1)-(2.4)) can be written in a matrix form:

$$\mathbf{A}(\mathbf{W})\partial_t\mathbf{W} + \mathbf{B}(\mathbf{W})\partial_{\mathbf{s}}\mathbf{W} - \mathbf{C}(\mathbf{W}) - \mathbf{D}(\mathbf{W})\partial_{ss}\mathbf{W} - \mathbf{E}(\mathbf{W})\partial_{sss}\mathbf{W} = 0. \tag{4.13}$$

To study linear stability,

$$\mathbf{A}(\mathbf{W})\partial_t\mathbf{W} + \mathbf{B}(\mathbf{W})\partial_{\mathbf{s}}\mathbf{W} - \mathbf{C}(\mathbf{W}) = 0, \tag{4.14}$$

where $\mathbf{W} = [\alpha_l, u_l, u_g, p]^T$ is a column vector of the variables. The governing equations were linearized around a reference state with an infinitesimally small perturbation imposed: $\mathbf{W} = \mathbf{W}_0 + \widetilde{\mathbf{W}}$.

$$\begin{aligned}\mathbf{A}(\mathbf{W}_0 + \widetilde{\mathbf{W}})\partial_t(\mathbf{W}_0 + \widetilde{\mathbf{W}}) + \mathbf{B}(\mathbf{W}_0 + \widetilde{\mathbf{W}})\partial_{\mathbf{s}}(\mathbf{W}_0 + \widetilde{\mathbf{W}}) \\ -\mathbf{C}(\mathbf{W} + \mathbf{W}_0) = 0,\end{aligned} \tag{4.15}$$

Linearizing the nonlinear terms $\mathbf{M} \in [\mathbf{A}, \mathbf{B}, \mathbf{C}]$ by means of Taylor expansions around its unperturbed value:

$$\mathbf{M}(\mathbf{W}_0 + \widetilde{\mathbf{W}}) = \mathbf{M}(\mathbf{W}_0) + (\partial_W \mathbf{M}(W))_{\mathbf{W}_0}\,\widetilde{\mathbf{W}} \tag{4.16}$$

equation (4.15) stands:

$$\begin{aligned}&\left[\mathbf{A}(\mathbf{W}_0) + (\partial_{\mathbf{W}}\mathbf{A}(\mathbf{W}))_{\mathbf{W}_0}\,\widetilde{\mathbf{W}}\right]\partial_t\mathbf{W}_0 \\ &+\left[\mathbf{A}(\mathbf{W}_0) + (\partial_{\mathbf{W}}\mathbf{A}(\mathbf{W}))_{\mathbf{W}_0}\,\widetilde{\mathbf{W}}\right]\partial_t\widetilde{\mathbf{W}} \\ &+\left[\mathbf{B}(\mathbf{W}_0) + (\partial_{\mathbf{W}}\mathbf{B}(\mathbf{W}))_{\mathbf{W}_0}\,\widetilde{\mathbf{W}}\right]\partial_{\mathbf{s}}\mathbf{W}_0 \\ &+\left[\mathbf{B}(\mathbf{W}_0) + (\partial_{\mathbf{W}}\mathbf{B}(\mathbf{W}))_{\mathbf{W}_0}\,\widetilde{\mathbf{W}}\right]\partial_{\mathbf{s}}\widetilde{\mathbf{W}} \\ &-\left[\mathbf{C}(\mathbf{W}_0) + (\partial_{\mathbf{W}}\mathbf{C}(\mathbf{W}))_{\mathbf{W}_0}\,\widetilde{\mathbf{W}}\right] = 0\end{aligned} \tag{4.17}$$

If the second-order terms (i.e., the product of disturbances) vanish, the linearized Two-fluid Model follows:

$$\begin{aligned}\mathbf{A}(\mathbf{W}_0)\partial_t\widetilde{\mathbf{W}} + \mathbf{B}(\mathbf{W}_0)\partial_{\mathbf{s}}\widetilde{\mathbf{W}} \\ +\left[(\partial_{\mathbf{W}}\mathbf{A}(\mathbf{W}))_{\mathbf{W}_0}\,\partial_t\mathbf{W}_0 + (\partial_{\mathbf{W}}\mathbf{B}(\mathbf{W}))_{\mathbf{W}_0}\,\partial_{\mathbf{s}}\mathbf{W}_0 - (\partial_{\mathbf{W}}\mathbf{C}(\mathbf{W}))_{\mathbf{W}_0}\right]\widetilde{\mathbf{W}} + \text{const},\end{aligned} \tag{4.18}$$

The column matrix is:

$$\mathbf{A}(\mathbf{W}_0) + \mathbf{B}(\mathbf{W}_0) - \mathbf{C}(\mathbf{W}_0) = 0. \tag{4.19}$$

APPENDIX 4 - TWO-FLUID MODEL CONSIDERING NUMERICAL DIFFUSION TERMS

The complete Two-fluid Model (i.e., Eqs. (2.1)-(2.4)), with gas compressibility (Bonizzi, 2003; Sanderse; Smith; Hendrix, 2017; Smith, 2017; Zwieten et al., 2017) and numerical viscosity (Bonzanini; Picchi; Poesio, 2017; Holmås et al., 2008; Montini, 2010) reads:

Continuity

$$\partial_t \left(\alpha_l \rho_l\right) + \partial_{\mathbf{s}} \left(\alpha_l \rho_l u_l\right) = \rho_l \Gamma_l \partial_{\mathbf{ss}} \alpha_l \tag{4.20}$$

$$\partial_t \left(\alpha_g \rho_g\right) + \partial_{\mathbf{s}} \left(\alpha_g \rho_g u_g\right) = \rho_g \Gamma_g \partial_{\mathbf{ss}} \alpha_g \tag{4.21}$$

Momentum

$$\begin{aligned} &\partial_t \left(\alpha_l \rho_l u_l\right) + \partial_{\mathbf{s}} \left(\alpha_l \rho_l u_l^2\right) + \alpha_l \partial_{\mathbf{s}} p_i + \alpha_l \rho_l D_c \partial_{\mathbf{s}} \alpha_l \\ &= -\alpha_l \rho_l g \sin\beta - \frac{\tau_{lw} P_{lw}}{A} - \frac{\tau_{gl} P_{gl}}{A} + \alpha_l \nu_l \partial_{\mathbf{ss}} u_l \end{aligned} \tag{4.22}$$

$$\begin{aligned} &\partial_t \left(\alpha_g \rho_g u_g\right) + \partial_{\mathbf{s}} \left(\alpha_g \rho_g u_g^2\right) + \alpha_g \partial_{\mathbf{s}} p_i - \alpha_g \rho_g D_c \partial_{\mathbf{s}} \alpha_g \\ &= -\alpha_g \rho_g g \sin\beta - \frac{\tau_{gw} P_{gw}}{A} + \frac{\tau_{gl} P_{gl}}{A} + \alpha_g \nu_g \partial_{\mathbf{ss}} u_g \end{aligned} \tag{4.23}$$

The corrected diameter D_c is expressed by (2.14). Equations (4.20) -(4.23) can be rewritten in terms of the primitive variables α_l, u_l, u_g, p_i as follows:

Continuity

$$\rho_l \partial_t \alpha_l + \rho_l \alpha_l \partial_{\mathbf{s}} u_l + \rho_l u_l \partial_{\mathbf{s}} \alpha_l - \rho_l \Gamma_l \partial_{\mathbf{ss}} \alpha_l = 0 \tag{4.24}$$

$$\begin{aligned} &\frac{1}{c_g^2}\left(1-\alpha_l\right) \partial_t p_i - \frac{1}{c_g^2} p_i \partial_t \alpha_l + \frac{1}{c_g^2}\left(1-\alpha_l\right) p_i \partial_{\mathbf{s}} u_g \\ &+\frac{1}{c_g^2}\left(1-\alpha_l\right) u_g \partial_{\mathbf{s}} p_i - \frac{1}{c_g^2} u_g p_i \partial_{\mathbf{s}} \alpha_l + \frac{1}{c_g^2} \Gamma_g p_i \partial_{\mathbf{ss}} \alpha_l = 0 \end{aligned} \tag{4.25}$$

Momentum

$$\begin{aligned} &\rho_l \alpha_l \partial_t u_l + \rho_l u_l \partial_t \alpha_l + 2\rho_l \alpha_l u_l \partial_{\mathbf{s}} u_l + \rho_l u_l^2 \partial_{\mathbf{s}} \alpha_l + \alpha_l \partial_{\mathbf{s}} p_i + \rho_l D_c \alpha_l \partial_{\mathbf{s}} \alpha_l \\ &+\rho_l g \sin\beta \alpha_l + \frac{\tau_{wl} P_{lw}}{A} + \frac{\tau_{gl} P_{gl}}{A} - \nu_l \alpha_l \partial_{\mathbf{ss}} u_l = 0 \end{aligned} \tag{4.26}$$

$$\begin{aligned} &\frac{1}{c_g^2}\left(1-\alpha_l\right) p_i \partial_t u_g + \frac{1}{c_g^2}\left(1-\alpha_l\right) u_g \partial_t p_i - \frac{1}{c_g^2} u_g p_i \partial_t \alpha_l + 2\frac{1}{c_g^2}\left(1-\alpha_l\right) u_g p_i \partial_{\mathbf{s}} u_g \\ &+\frac{1}{c_g^2}\left(1-\alpha_l\right) u_g^2 \partial_{\mathbf{s}} p_i - \frac{1}{c_g^2} u_g^2 p_i \partial_{\mathbf{s}} \alpha_l + \left(1-\alpha_l\right) \partial_{\mathbf{s}} p_i + \frac{1}{c_g^2} D_c \left(1-\alpha_l\right) p_i \partial_{\mathbf{s}} \alpha_l \\ &+\frac{1}{c_g^2} g \sin\beta \left(1-\alpha_l\right) p_i + \frac{\tau_{gw} P_{gw}}{A} - \frac{\tau_{gl} P_{gl}}{A} - \nu_g \left(1-\alpha_l\right) \partial_{\mathbf{ss}} u_g = 0 \end{aligned} \tag{4.27}$$

The matrices $\mathbf{A}$, $\mathbf{B}$, $\mathbf{C}$ and $\mathbf{D}$ are:

$$\mathbf{A} = \begin{pmatrix} \rho_l & 0 & 0 & 0 \\ -\frac{1}{c_g^2} p_i & 0 & 0 & \frac{1}{c_g^2}\left(1-\alpha_l\right) \\ \rho_l u_l & \rho_l \alpha_l & 0 & 0 \\ -\frac{1}{c_g^2} u_g p & 0 & \frac{1}{c_g^2}\left(1-\alpha_l\right) p_i & \frac{1}{c_g^2}\left(1-\alpha_l\right) u_g \end{pmatrix} \tag{4.28}$$

$$\mathbf{B} = \begin{pmatrix} \rho_l u_l & \rho_l \alpha_l & 0 & 0 \\ -\frac{1}{c_g^2} u_g p & 0 & \frac{1}{c_g^2}\left(1-\alpha_l\right) p_i & \frac{1}{c_g^2}\left(1-\alpha_l\right) u_g \\ \rho_l u_l^2 + \rho_l D_c \alpha_l & 2\rho_l \alpha_l u_l & 0 & \alpha_l \\ -\frac{1}{c_g^2} u_g^2 p_i + \frac{1}{c_g^2} D_c \left(1-\alpha_l\right) p_i & 0 & \frac{1}{c_g^2} 2\left(1-\alpha_l\right) u_g p_i & \frac{1}{c_g^2}\left(1-\alpha_l\right) u_g^2 + \left(1-\alpha_l\right) \end{pmatrix} \tag{4.29}$$

$$\mathbf{C} = \begin{pmatrix} 0 \\ 0 \\ -\rho_l g \sin\beta \alpha_l A - \tau_{lw} P_{lw} - \tau_{gl} P_{gl} \\ -\frac{1}{c_g^2} g A \sin\beta \left(1-\alpha_1\right) p_i - \tau_{gw} P_{gw} + \tau_{gl} P_{gl} \end{pmatrix} \tag{4.30}$$

$$\mathbf{D} = \begin{pmatrix} \rho_l \Gamma_l & 0 & 0 & 0 \\ -\frac{1}{c_g^2} \Gamma_g p_i & 0 & 0 & 0 \\ 0 & \alpha_l \nu_l & 0 & 0 \\ 0 & 0 & \left(1-\alpha_l\right) \nu_g & 0 \end{pmatrix} \tag{4.31}$$

ANNEX 1 - 11TH INTERNATIONAL CONFERENCE ON MULTIPHASE FLOW, KOBE, JAPAN. 2023

78

Prediction of flow pattern transition in pipelines using Taylor-Hood finite elements

David Lazo-Vásquez and Jorge Luis Baliño

Universidade de São Paulo, Escola Politécnica, Departmento de Engenharia Mecânica

Av. Professor Mello Moraes, São Paulo, 2231, Brazil

lazovasquez@usp.br, jlbalino@usp.br

Keywords: gas-liquid flow, two-fluid model, Taylor-Hood elements, stability, wave growth prediction

Abstract

Stratified to intermittent flow pattern transition modeling is particularly interesting for production assurance in large oil and gas systems. In long pipes, the one-dimensional two-fluid model has been employed to predict wave growth, despite its conditional well-posedness for high phasic velocities and excessive numerical diffusion that can attenuate physical disturbances. This work investigates wave growth and flow pattern transition prediction of gas-liquid flows. The compressible one-dimensional two-fluid model is solved using implicit time schemes and Taylor-Hood finite elements for spatial discretization, satisfying the inf-sup stability and circumventing the use of staggered grids. Simultaneously, the numerical formulation tracks the effective stability of the fluid flow with the aid of the construction of fully discrete flow pattern maps in time. In conclusion, for unstable initial conditions, the numerical formulation predicts wave growth along the pipe with a stratified smooth flow as the initial condition. Also, the potential transition to intermittent flow is predicted when imposing an infinitesimal perturbation in the form of a sinusoidal wave.

Introduction

In oil and gas systems, multiphase flows present various phasic distributions in pipelines depending on several factors (e.g., phasic velocities, pipe diameter, and local inclination). In long pipes, the one-dimensional two-fluid model has been employed to predict flow pattern transitions although its conditional well-posedness, resolving it through different numerical formulations (i.e., finite differences, finite volume, and finite elements).

Most codes used by the petroleum industry resolve the two-fluid model with first-order discretization schemes for the convection terms. Also, some employ *ad hoc* artificial diffusion to attenuate the numerical instabilities innate to the ill-posedness nature of the two-fluid model equations at high flow rates. However, most methods lead to non-monotone results and are limited to lower-order numerical schemes and straight pipes.

This work aims to resolve the compressible one-dimensional two-fluid model (hereafter two-fluid model) with Taylor-Hood finite elements and implicit time schemes, using the slug capturing methodology introduced by Issa and Kempf (2003) as a reference. The equations are numerically solved simultaneously with the construction of fully-discrete flow pattern maps, previously introduced by Sanderse et al. (2017), to facilitate tracking wave growth and stability in time. The code, implemented in the Python 3 language, using the FEniCS Project Platform, is available online (Lazo-Vasquez and Baliño 2022).

Methods

Governing equations and closure relations: The two-fluid model of Ishii and Hibiki (2010) for isothermal flow consists of a set of mass and momentum conservation equations for the gas and liquid phases:

$$\partial_t \left(\alpha_k \rho_k\right) + \partial_s \left(\alpha_k \rho_k u_k\right) = 0 \tag{1}$$

$$\begin{aligned} \partial_t \left(\alpha_k \rho_k u_k\right) + \partial_s \left(\alpha_k \rho_k u_k^2\right) + \alpha_k \partial_s p_i + \\ \alpha_k \rho_k g \partial_s h_i \cos\beta = -\alpha_k \rho_k g \sin\beta - \\ \sum_{\theta \in \{l,g,w\}} \frac{\tau_{k\theta} P_{k\theta}}{A} \end{aligned} \tag{2}$$

The subscript $k \in \{l, g\}$) represents the liquid and gas phases, w the pipe wall, and i the interface. The liquid and gas volume fractions satisfy $\alpha_l + \alpha_g = 1$. The local inclination angle is denoted by β. The wetted perimeter P and shear stress terms τ are modeled by the combination proposed by Issa and Kempf (2003).

Spatial and time discretization: Equations (1) and (2) are simultaneously approximated by the variational form:

$$\begin{aligned} \sum_{\Omega \in \Omega_h} \int_\Omega \left(\partial_t \mathbf{W}_h \, \mathbf{V} \, + \mathbf{V}.\nabla \mathbf{B}_h \, \mathbf{W}_h \, \right) \mathrm{d}x \\ = \sum_{\Omega \in \Omega_h} \int_\Omega \mathbf{C}_h \, \mathrm{d}x \end{aligned} \tag{3}$$

where $\mathbf{W}_h\left(s,t\right) = \left[\alpha_l, u_l, u_g, p_i\right]^{\mathrm{T}} \in \mathbb{R}^{q=4}$ represents the vector of the discretized variables (i.e., liquid volume frac-

tion, liquid and gas velocities, and interfacial pressure), $\mathbf{B}_h$ the Jacobian matrix, $\mathbf{C}_h$ the source terms vector, $\Omega \subset \mathbb{R}^n$ the spatial domain containing n elements, and $\mathbf{W_h}$ and $\mathbf{V}$ the trial and test function vectors.

The convective and source terms are discretized with Taylor Hood $\mathcal{P}_2-\mathcal{P}_1$ mixed elements, consisting of second-order Continuous Galerkin (CG) elements for u_l and u_g, and first-order CG for α_l and p_i, circumventing the use of staggered grids. The time derivatives are discretized with BDF2.

Results and discussion

As the first approach, we simulate air-water flow ($\rho_l = 1000$ kg/m^3, $\mu_l = 1.8e-5$ Pa s, $\mu_g = 8.9e-4$ Pa s) in a horizontal pipe with $D = 0.078$ m, $L = 1$ m, and $n = 360$ elements.

Linear wave growth: Wave growth simulations and the construction of fully-discretized flow pattern maps (see Fig. 1) are performed simultaneously to track the stability of the equations within the entire domain. The linearized equations

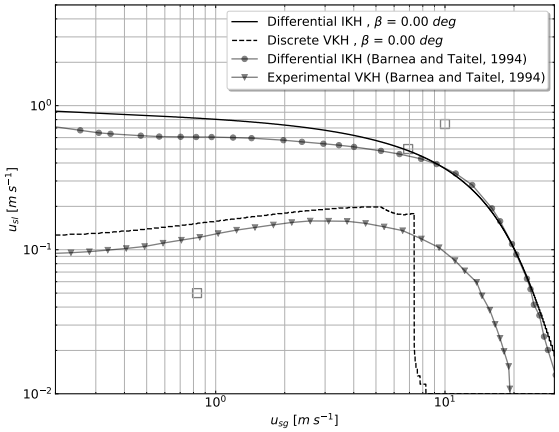

Figure 1: Fully-discrete flow pattern map for the studied conditions, validated with the maps of Barnea and Taitel (1994).

are solved for the phasic velocities $u_{sl} = 0.5$ m/s and $u_{sg} = 6.908$ m/s, located in the unstable region (Fig. 2).

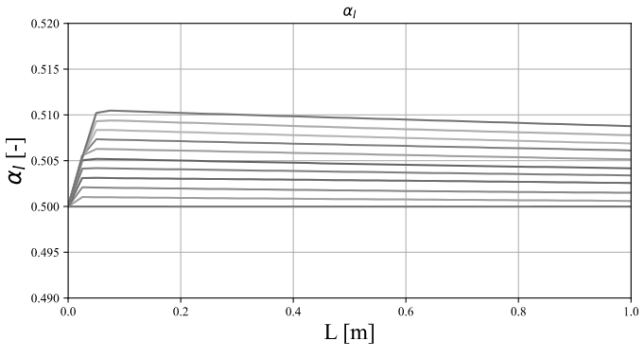

Figure 2: Liquid holdup α_l variation during linear wave growth simulations of an unstable flow.

Nonlinear wave growth: Imposing a sinusoidal perturbation ($k = 2\pi$ 1/m and $\omega = 8.484$ 1/s), the liquid holdup grows in time until blocking the pipe (Fig. 3). The equations become ill-posed, and a correlation for the flow pattern switch can be used for the solution.

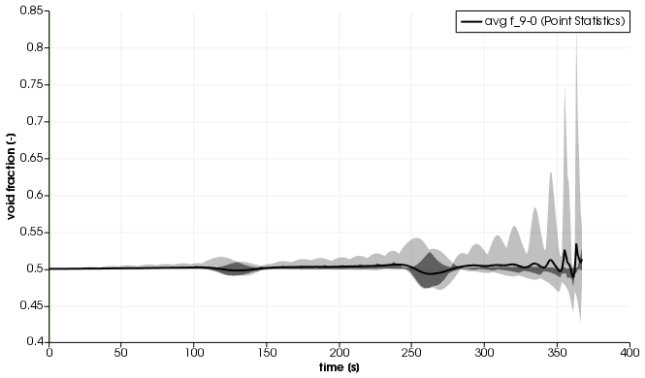

Figure 3: Void fraction α_g variation at the pipe outlet ($s = 1$ m) due to wave growth after imposing a sinusoidal perturbation.

Conclusions

The numerical formulation predicts potential flow pattern transitions due to wave growth in stratified flows with unstable initial conditions.

Simultaneous nonlinear simulations and fully-discrete flow pattern map construction facilitate tracking stability in the entire spatial domain, independently of the local pipe inclination.

Acknowledgments

This work was supported by *Coordenação de Aperfeiçoamento de Pessoal de Nível Superior* (CAPES), *Fundação de Desenvolvimento Tecnológico da Engenharia* (FDTE), *Conselho Nacional de Desenvolvimento Científico e Tecnológico* (CNPq), and *Petróleo Brasileiro S.A.* (Petrobras).

References

D. Barnea and Y. Taitel. Interfacial and structural stability of separated flow. *International Journal of Multiphase Flow*, 20:387–414, 1994.

Mamoru Ishii and Takashi Hibiki. Thermo-fluid dynamics of two-phase flow, 2010.

R. I. Issa and M. H. W. Kempf. Simulation of slug flow in horizontal and nearly horizontal pipes with the two-fluid model. *International Journal of Multiphase Flow*, 29(1):69–95, 2003.

D. Lazo-Vasquez and J. L Baliño. Sample code for ICMF 2023 v1.1. *GitHub Repository*, 2022. doi: 10.5281/zenodo.7044602.

B. Sanderse, I. E. Smith, and M. H.W. Hendrix. Analysis of time integration methods for the compressible two-fluid model for pipe flow simulations. *International Journal of Multiphase Flow*, 95:155–174, 2017.

ANNEX 2 - JOURNAL OF THE BRAZILIAN SOCIETY OF MECHANICAL SCIENCES AND ENGINEERING SUBMISSION PAGE

Journal of the Brazilian Society of Mechanical Sciences and Engineering

On the use of Taylor-Hood elements for dynamic simulations of gas-liquid flows using the two-fluid model

--Manuscript Draft--

Manuscript Number:	
Full Title:	On the use of Taylor-Hood elements for dynamic simulations of gas-liquid flows using the two-fluid model
Article Type:	S.I. : CBCFD 2022 (by invitation only)
Section/Category:	Fluid mechanics
Funding Information:	Conselho Nacional de Desenvolvimento Científico e Tecnológico — Dr Jorge Luis Baliño Coordenação de Aperfeiçoamento de Pessoal de Nível Superior — Mr David Lazo-Vasquez Fundação para o Desenvolvimento Tecnológico da Engenharia (FDTE) — Mr David Lazo-Vasquez
Abstract:	In the oil and gas industry, predicting flow pattern transitions is essential in sizing pipelines and receiving facilities. The one-dimensional two-fluid model is employed for simulating two-phase flows in long pipes; however, unexpected numerical diffusion can attenuate physical perturbations depending on the numerical formulation. This work presents a novel formulation for predicting liquid wave growth in pipelines with diverse local inclinations, with a stratified smooth flow as an initial condition. The equations are discretized with Taylor-Hood finite elements and implicit time schemes. The eigenspectra of the semi-discrete equations prove the capability of the numerical method to describe wave growth for different initial conditions, mesh configurations, and local pipe inclinations. Also, the eigenspectra show that the convective modes contribute to instability and consequent wave growth for unstable initial conditions. Finally, the fully discrete Kelvin-Helmholtz-based flow pattern maps depict the effective stability regions for a large set of initial conditions. The capability of the formulation for describing wave growth, demonstrated through eigenspectra and flow pattern maps, agrees with the experimental and theoretical data from the literature. Overall, due to the ease of adding regularization terms, increasing the order of basis functions, and modifying the pipe geometry, the numerical formulation can predict wave growth leading to flow pattern transitions under different conditions.
Corresponding Author:	David Lazo-Vasquez Universidade de São Paulo Sao Paulo, SP BRAZIL
Corresponding Author Secondary Information:	
Corresponding Author's Institution:	Universidade de São Paulo
Corresponding Author's Secondary Institution:	
First Author:	David Lazo-Vasquez
First Author Secondary Information:	
Order of Authors:	David Lazo-Vasquez Jorge Luis Baliño, Dr
Order of Authors Secondary Information:	
Author Comments:	The authors of this manuscript attended the III CBCFD and were invited to submit an extended congress manuscript to this special issue.

ANNEX 3 - III CONGRESSO BRASILEIRO DE FLUIDODINÂMICA, CAMPINAS, BRAZIL. 2022

III Congresso Brasileiro de Fluidodinâmica Computacional
20 a 22 de Julho de 2022
Campinas - SP

ON THE USE OF CONTINUOUS FINITE-ELEMENTS FOR TWO-PHASE FLOW SIMULATIONS IN HORIZONTAL AND NEARLY HORIZONTAL PIPES

D. LAZO-VÁSQUEZ [1] E J. L. BALIÑO[2]

[1,2] Universidade de São Paulo, Escola Politécnica, Departamento de Engenharia Mecânica

Email para contato: lazovasquez@usp.br

RESUMO – The one-dimensional two-fluid model, employed for simulating two-phase flows in long pipes, is conditionally well-posed and discretized with lower-order space and time schemes. This work investigates the capability of continuous finite-element methods of describing wave growth and potential flow pattern transitions, with stratified smooth flow as an initial condition, using the FEniCS computing platform. The effects of initial conditions, mesh configuration, order of basis functions, and pipe inclination on the stability were investigated through eigenspectra and flow pattern maps of the differential and discrete equations. The numerical model proposed describes potential wave growth, which serves as a baseline for simulating flow pattern transitions in oil and gas systems.

1. INTRODUCTION

Two-phase flows in long pipes are frequently simulated with the one-dimensional two-fluid model (hereafter two-fluid model), proposed by Ishii e Hibiki (2011). In large systems, the pipe lengths are of the order of kilometers and gas bubble diameters of millimeters van Zwieten et al. (2017).

Issa e Kempf (2003) proposed the slug capturing approach by solving the two-fluid model under well-posed initial conditions, simulating the natural growth of instabilities starting from non-equilibrium flows. Issa e Kempf (2003); Liao et al. (2008) used first-order Finite Volume central schemes to avoid excessive numerical diffusion associated with upwind schemes.

This paper proposes a methodology for predicting potential wave growth, solving the two-fluid model. We investigate the spatial discretization with Continuous Galerkin and Taylor-Hood finite elements, often employed for solving the Navier-Stokes equations and other convection-dominated problems Logg et al. (2012).

2. METHODS

The starting point of this work is the slug capturing approach of Issa e Kempf (2003) and the equations of Montini (2010), with stratified smooth flow (see Fig. **??**) as the initial condition, as in the studies Sanderse et al. (2017); van Zwieten et al. (2017).

2.1. Governing equations

The two-fluid model Ishii e Hibiki (2011) consists of a set of transport equations for the phases, including mass, momentum, and energy equations. For isothermal flow, the

energy equations are dismissed Issa e Kempf (2003). The governing equations for one-dimensional stratified and slug flow read

$$\partial_t \left(\alpha_k \rho_k\right) + \partial_s \left(\alpha_k \rho_k u_k\right) = 0, \tag{1}$$

and

$$\partial_t \left(\alpha_k \rho_k u_k\right) + \partial_s \left(\alpha_k \rho_k u_k^2\right) + \alpha_k \partial_s p_i + \alpha_k \rho_k g \partial_s h_i \cos\beta = -\alpha_k \rho_k g \sin\beta - \sum_{\theta \in \{l,g,w\}} \frac{\tau_{k\theta} P_{k\theta}}{A}, \tag{2}$$

where $\theta \neq k$, w is the pipe wall. The liquid and gas volume fractions sum to one ($\alpha_l + \alpha_g = 1$). The liquid, gas, and interface are represented by the subscripts l, g and i, respectively.

2.2. Spatial discretization

The convective terms of equations (1)-(2) should be carefully discretized to prevent issues related to numerical oscillations De Bertodano et al. (2016); Liao et al. (2008); Sanderse et al. (2017).

Equation (**??**) is simultaneously approximated by the variational form of Eq. (**??**):

$$\sum_{\Omega \in \Omega_h} \int_\Omega \partial_t \mathbf{W}_h \, \mathbf{V} \, \mathrm{d}x + \sum_{\Omega \in \Omega_h} \int_\Omega a_A \left(\mathbf{B_0}_{,h}; \mathbf{W}_h, \mathbf{V}\right) \mathrm{d}x = \sum_{\Omega \in \Omega_h} \int_\Omega \mathbf{C_0}_{,h} \, \mathrm{d}x, \tag{3}$$

where $\mathbf{W_h}$ and $\mathbf{V}$ are the vectors of trial and test functions, respectively. The convective term is denoted by a_A. $\Omega \subset \mathbb{R}^n$ is the spatial domain with boundaries $\partial\Omega = \Gamma_D^{in} \cup \Gamma_D^{out}$. At the inlet $\{\alpha_{l,0}, u_{l,0}, u_{g,0}\} \in \Gamma_D^{in}$, and at the outlet $\{p_{i,0}\} \in \Gamma_D^{out}$.

3. RESULTS AND DISCUSSION

The results are reported through eigenspectra and flow pattern maps, validated against the literature. To ease validation of the results, the input parameters are the same as Issa e Kempf (2003); Montini (2010); Sanderse et al. (2017). c_g is taken such that for $p_i = p_{i,0}$, the gas density $\rho_g = 1.1614\ kg\ m^{-3}$ Sanderse et al. (2017).

3.1. Stiffness analysis of the semi-discrete equations

Using Taylor-Hood elements, the existence of convective modes suggest that certain solutions might potentially grow in time, since they have a positive real part. Differently, using continuous elements, the eigenspectrum is composed of acoustic modes. The imaginary parts of the eigenvalues associated with acoustic and convective waves have different orders of magnitude since acoustic modes have higher frequencies than convective modes. Taylor-Hood function spaces preserve the eigenstructure for the parameters studied, suggesting the capability of such function spaces for describing wave growth.

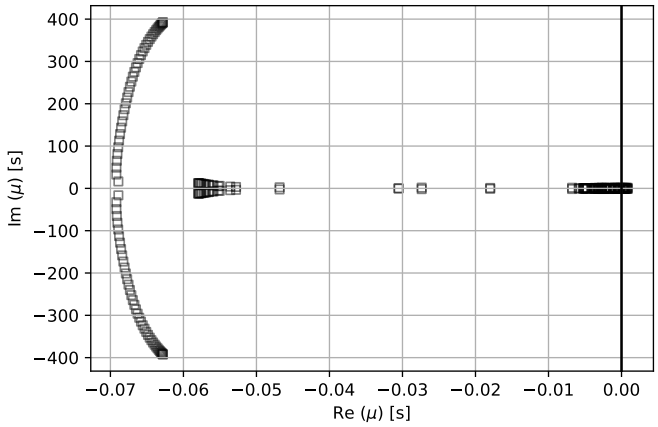

Figura 1 – Taylor-Hood P_2.

3.2. Discrete flow pattern maps

The VKH limits for the fully discrete equations are built with a sequence of superficial velocities, for the time step $\Delta t = 1/40$ as the first approach (See Fig. 2).

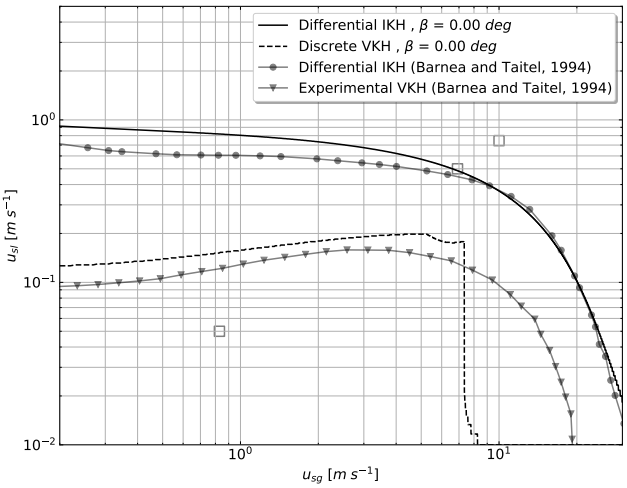

Figura 2 – Discrete flow pattern maps ($D = 0.051\ m$). Taylor-Hood P_2 combined with BDF2.

4. CONCLUSIONS

The stiffness analysis of the semi-discretized equations reveals the influence of pipe inclination on the presence of eigenvalues related to acoustic and convective waves. Convective waves are not attenuated by numerical diffusion present in the numerical schemes. The eigenvalues associated with acoustic waves do not affect the wave growth for smooth initial conditions. Continuous finite element function spaces represent alternatives to solve the two-fluid model equations under smooth initial conditions. Additionally, the discretization with Taylor-Hood mixed finite elements, combined with implicit time schemes, describes potential wave growth.

Discrete flow pattern maps for different pipe inclinations validate the numerical methods proposed during the first time steps in transient simulations. Differential and discrete flow pattern maps based on Kelvin-Helmholtz instabilities present good agreement with experimental data available in the literature. Meanwhile, it is essential to simultaneously validate the actual flow patterns and transition curves through differential flow pattern maps, discrete flow pattern maps, and nonlinear simulations.

5. REFERÊNCIAS

De Bertodano, M. L.; Fullmer, W.; Clausse, A.; Ransom, V. H. *Two-fluid model stability, simulation and chaos*. Springer, 2016.

Ishii, M.; Hibiki, T. *Thermo-fluid dynamics of two-phase flow (Second edition)*. Springer Science \& Business Media, 2011.

Issa, R. I.; Kempf, M. H. Simulation of slug flow in horizontal and nearly horizontal pipes with the two-fluid model. *International Journal of Multiphase Flow*, 29(1), 69–95, 2003.

Liao, J.; Mei, R.; Klausner, J. F. A study on the numerical stability of the two-fluid model near ill-posedness. *International Journal of Multiphase Flow*, 34(11), 1067–1087, 2008.

Logg, A.; Mardal, K. A.; Wells, G. *Automated Solution of Differential Equations by the Finite Element Method: The FEniCS Book (Lecture Notes in Computational Science and Engineering)*, volume 84. Springer Science & Business Media, 2012.

Montini, M. Closure relations of the one-dimensional two-fluid model for the simulation of slug flows. *October*, (October), 241, 2010.

Sanderse, B.; Smith, I. E.; Hendrix, M. H. Analysis of time integration methods for the compressible two-fluid model for pipe flow simulations. *International Journal of Multiphase Flow*, 95, 155–174, 2017.

van Zwieten, J. S.; Sanderse, B.; Hendrix, M. H.; Vuik, C.; Henkes, R. A. Efficient simulation of one-dimensional two-phase flow with a high-order h-adaptive space-time Discontinuous Galerkin method. *Computers and Fluids*, 156, 34–47, 2017.

ANNEX 4 - 10TH INTERNATIONAL CONFERENCE ON MULTIPHASE FLOW, RIO DE JANEIRO, BRAZIL. 2019

90

Sample-based prior using a phenomenological model for slug flow

Sergio P. Pellegrini, David Lazo-Vásquez, Flávio C. Trigo,
Raul G. Lima and Jorge L. Baliño

Universidade de São Paulo, Escola Politécnica, Departamento de Engenharia Mecânica

Av. Prof. Mello Moraes 2231, São Paulo, 05508-030 Brazil

sergio.pellegrini@gmail.com, david.lazo@usp.br, trigo.flavio@usp.br, rauglima@usp.br, jlbalino@usp.br

Keywords: slug flow, gas-liquid flow, electrical impedance tomography, sample-based prior

Abstract

Among the techniques for multiphase flow monitoring, Electrical Impedance Tomography (EIT) allows for non-intrusive measurement but is hindered by its intrinsic ill-posed characteristics. One form of dealing with this challenge is the introduction of prior knowledge, such as flow pattern. This work presents the design of a library for EIT grounded on a literature-based phenomenological model. An adapted mechanistic model of gas-liquid slug flow is constructed to provide the disposition of the phases departing from fluid properties, geometrical parameters and flow conditions. This is accomplished with a unit-cell model for slug flow and a statistical slug length prediction method. Sampling of different flow conditions, along with sampling of the expected deviations of the correlations implemented, is used to obtain a phase distribution in the continuum. Electrical properties are attributed for both phases and, with a finite mesh, a series of representative images are numerically obtained for slug flow. Results are presented treating the distribution as a Gaussian density function. This library is expected to support the regularization of the inverse EIT problem, in the sense of a Bayesian prior.

Introduction

EIT allows for non-intrusive estimation of phase distribution, as electric properties in a duct can be calculated from the electric currents imposed on electrodes at the duct wall and the resulting measured electric potentials. This problem is mathematically ill-posed, as sensor noise prevents the inversion of the data to obtain a unique image for the flow. One single solution can, though, be achieved with the introduction of priorly know information from sources other than the measured data.

A typical information that can be imposed is that the solution is smooth. For this case, a single solution is reached at the expense of blurring the estimated image.

Alternatively, sample-based Bayesian priors (Kaipio and Somersalo 2004, p.70) can be generated from a collection of images, described in terms of the electric properties. This library of images can be built with the support of other experimental techniques or through analytic models. This sample-based prior can provide a sharper image with finer details (Camargo 2013).

In the literature of multiphase systems, there are many analytic models to predict phase distribution characteristic behaviors, depending on the flow pattern. A sample-based library from a phenomenological model for annular flow was presented in Pellegrini et al. (2016). However, as intermittent flow is of particular interest for the oil industry, this work aims at constructing a library of slug flow based on a phenomenological model, to be used as a sample-based prior.

Numerical Methods

For this purpose, a phenomenological model was assembled combining correlations and equations from the literature. This model provides a characterization phase distribution within the continuum.

Next, a discrete (finite element) mesh is introduced, and values of electrical conductivity are attributed depending on the phase present near the centroid of each element.

Sampling values for superficial velocities, correlation errors, slug lengths and electrical conductivities, a library of images is obtained, providing a series of expected solutions for the estimation problem. This library is summarized in a Gaussian distribution, with the description in terms of a sample mean and covariance.

Phenomenological Model

The hydrodynamic average flow characteristics and the local holdup profiles were determined with the Unit-cell approach proposed by Taitel and Barnea (1990), as shown in Fig.1. The slug length was estimated by a log-normal distribution according to studies of Barnea and Taitel (1993) and Cook and Behnia (2000).

Transport equations: The mass and momentum equations proposed by Taitel and Barnea (1990) were used for computing the flow parameters. The combined momentum differential equation was solved numerically for the profile $h_f(z)$.

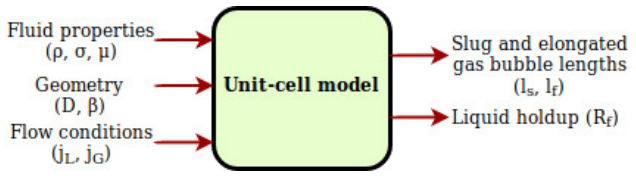

Figure 1: Unit-cell model parameters.

Closure models: The shear stress terms were modeled by the correlations of Taitel, Y. and Dukler (1976).

Results and Discussion

The phase occupation obtained through the phenomenological model and the discrete mesh is shown in Fig. 2, for four parts of the unit cell. The use of a short mesh (to model the influence of the electrodes) does not prevent the representation of the complete unit cell.

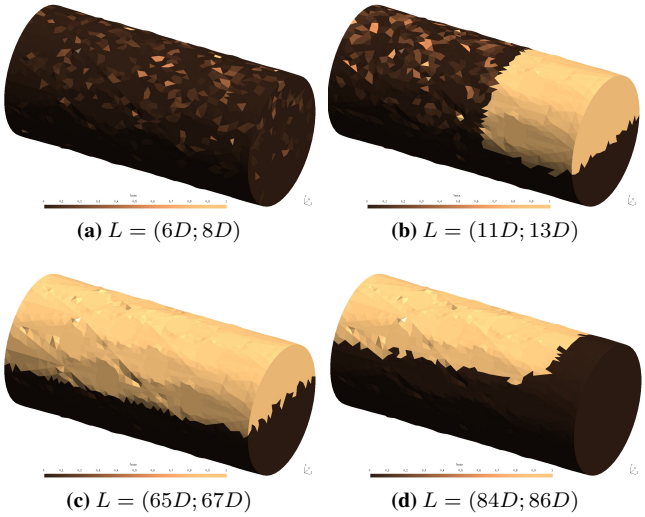

(a) $L = (6D; 8D)$ **(b)** $L = (11D; 13D)$

(c) $L = (65D; 67D)$ **(d)** $L = (84D; 86D)$

Figure 2: Representative images for one unit cell, in terms of phase occupation with air (bright color) and water (dark): (a) body of the slug, (b) upstream end of the slug and bubble tail, (c) body of the bubble and (d) bubble nose.

The obtained sample mean is shown in Fig. 3.

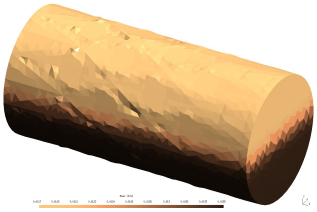

Figure 3: Sample mean ($N = 486620$ images generated), in terms of electrical conductivity.

With the eigenvalue decomposition of the covariance matrix, the two most important directions of variation are shown in Fig. 4. These seem coherent with the properties of a slug flow, as the first eigenvector can denote the passage of a slug and the second, the variation of the height of the film.

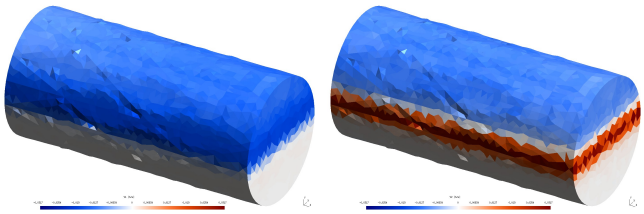

(a) Eigenvalue, $\lambda_1 = 1.610^3$ **(b)** Eigenvalue, $\lambda_2 = 4.610^4$

Figure 4: Most important eigenvectors of the empirical covariance matrix calculated ($N = 486620$).

Conclusions

Unit-cell modelling is shown to be an efficient computational approach to characterize the local phase distribution in slug flow.

The resulting library is compatible with the behavior of slug flow and can help obtaining more accurate EIT estimates.

Acknowledgments

The authors are thankful for the support of Petrobras, Agência Nacional do Petróleo, Gás Natural e Biocombustíveis (ANP, Brazil), Conselho Nacional de Desenvolvimento Científico e Tecnológico (CNPq, Brazil) and Coordenação de Aperfeiçoamento de Pessoal de Nível Superior (CAPES, Brazil).

References

Barnea, D. & Taitel, Y. A model for slug length distribution in gas-liquid slug flow. Int. J. Multiphase Flow, Vol. 19, pp. 829–838, (1993)

Camargo, E. D. L. B. Desenvolvimento de algoritmo de imagens absolutas de tomografia por impedância elétrica para uso clínico (PhD thesis). Escola Politécnica da Universidade de São Paulo, (2013)

Cook, M. & Behnia, M. Slug length prediction in near horizontal gas-liquid intermittent flow. Chemical Engineering Science, Vol. 55, pp. 2009–2018, (2000)

Kaipio, J. & Somersalo, E. Statistical and Computational Inverse Problems. Springer-Verlag, (2004)

Pellegrini, S. P. & Baliño, J. L. & Trigo, F. C. Design of a sample-based prior using a phenomenological model for annular flow. Proceedings of the 8th World Congress on Industrial Process Tomography, Iguassu Falls, Brazil, (2016)

Taitel, Y. & Dukler, A. E. A model for predicting flow regime transitions in horizontal and near horizontal gas-liquid flow. AIChE journal, Wiley Online Library, pp. 47–55, (1976)

Taitel, Y. & Barnea, D. Two-Phase Slug Flow. In Advances in heat transfer, Vol. 20, pp. 83-132. Elsevier, (1990)